ISSN 1818-2712
J Nucl Med Tech
核 醫 技 學 誌

核醫技術學雜誌

Journal of Nuclear Medicine Technology

Journal of Nuclear Medicine Technology
核醫技術學雜誌

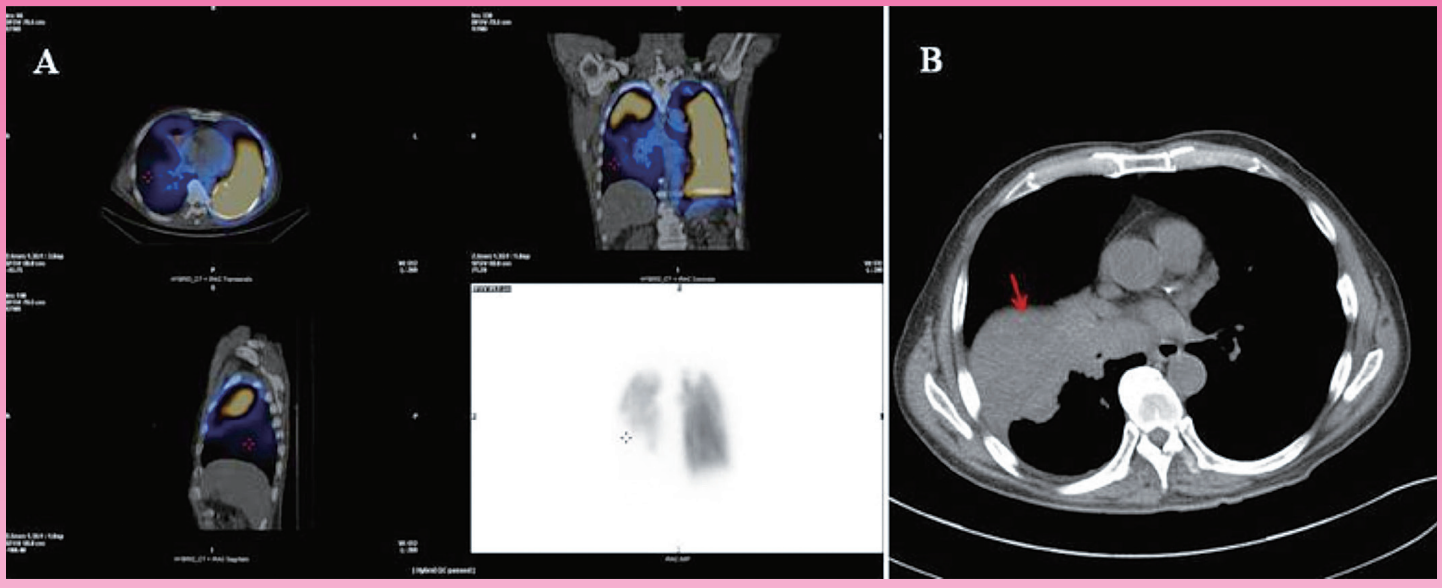

SPECT/CT images revealed possible cancer-induced right lower lung perfusion defect; therefore PE could not be excluded (Fig. A). CT image shows a large right lower lobe mass invading the right lower lobe bronchus and right inferior pulmonary vein, comparable to the malignant neoplasm of the lower lobe, right bronchus, or lung (red arrow in Fig. B). Therefore, the perfusion defect was probably secondary to the tumoral invasion of the pulmonary vessels, and PE was less likely.

Volume 17 Number 1 December 2020

第十七卷 第一期 中華民國一〇九年十二月

Published by NM Technology Committee, the Society of Nuclear Medicine, R.O.C.

中 華 民 國 核 醫 學 學 會

醫 技 委 員 會 發行

Volume 17 Number 1 Pages 1-44 December 2020

核醫技術學雜誌
Journal of Nuclear Medicine Technology

核醫技術學雜誌

第 17 卷第 1 期　　中華民國核醫學學會醫技委員會學誌　　中華民國 109 年 12 月發行

原　著

^{18}F-FDG PET/CT 在子宮頸癌的臨床價值 …… 1
柴發順　江泰林　歐玲君　李正輝

以蒙地卡羅模擬實驗展示鉛衣屏蔽效果…… 19
柴發順　江泰林　歐玲君　李正輝

病例報告

子宮肌瘤在 ^{99m}Tc-MDP 全身骨骼掃描與 SPECT/CT 影像上表現：
兩位病例報告…… 29
朱秀蘭　游慧貞　宋純穎　莊雅雯　劉芝庭

透過 SPECT/CT 於 ^{99m}Tc-MAA 肺灌注檢查證實肺癌侵犯所導致缺損之影像 …… 33
郭俊良　張鈺弘

曾有肋間手術史患者因手臂定位而導致 PET/CT 胸部偽陽性…… 39
吳麗君　顏玉安　李將瑄

Journal of Nuclear Medicine Technology

The Official Publication of NM Technology Committee, the Society of Nuclear Medicine, R.O.C.

ISSN 1818-2712

Volume 17, Number 1 December 2020

Original Articles

Clinical Value of ^{18}F-FDG PET/CT in Cervical Cancer 1
Fa-Shun Tsai, Tai-Lin Jiang, Lin-Chun Ou, Cheng-Hui Lee

The Demonstration of the Radiation Shielding Ability of Lead Apron: A Monte Carlo Simulation Experiment 19
Fa-Shun Tsai, Tai-Lin Jiang, Lin-Chun Ou, Cheng-Hui Lee

Case Reports

^{99m}Tc-MDP Bone Scintigraphy and SPECT/CT Manifestations in Patient with Leiomyoma of the Uterus: A Report of Two Cases 29
Hsiu-Lan Chu, Hui-Chen Yu, Chun-Ying Sung, Ya-Wen Chuang, Chih-Ting Liu

Cancer Related Pulmonary Perfusion Defect Demonstrated by Tc-99m Macroaggregated Albumin Single-Photon Emission Computerized Tomography (SPECT)/Computed Tomography (CT) 33
Chun-Liang Kuo, Yu-Hung Chang

False Positive Chest PET/CT Due to Arm Positioning in Patients with A History of Intercostal Surgery 39
Li-Chun Wu, Yu-An Yen, Chiang-Hsuan Lee

中華民國 93 年 11 月 20 日創刊

發　　行：中華民國核醫學學會
　　秘　書　處

理　事　長：顏 若 芳

醫技委員會
主 任 委 員：杜 高 瑩

執 行 祕 書：王 秀 珊

會　　址：100 台北市中正區中山南路 7 號
　　台大醫院核醫部轉核醫學學會
電　　話：02-23562481
傳　　真：02-23957855
電子信箱：tsnm.tw@gmail.com
劃撥帳號：19781819
戶　　名：中華民國核醫學學會
印　　刷：宇晨企業有限公司 yuchen68@ms51.hinet.net
地　　址：台北市和平東路二段 151 號 6 樓
電　　話：(02) 27037667　傳真：27033381

^{18}F-FDG PET/CT 在子宮頸癌的臨床價值

柴發順* 江泰林 歐玲君 李正輝

新光吳火獅紀念醫院正子中心

中文簡介

子宮頸癌是常見的婦女癌症。子宮頸癌是全球女性第四大常見的癌症原因。本篇研究的目的在於介紹子宮頸癌並概括敘述 ^{18}F-FDG PET/CT 在子宮頸癌診斷及治療中的臨床價值。

子宮頸癌的分期系統除了常見的 TNM 分類系統，另一廣泛被使用的分期系統爲國際婦產科聯合會的 FIGO 系統。因爲淋巴結轉移對治療和預後有重大影響，近期 FIGO 分期將淋巴結轉移納入分期系統。在子宮頸癌初期，MRI 與 CT 表現出相當良好的敏感度與準確性，^{18}F-FDG PET/CT 由於軟組織分辨度不佳及受到尿液放射性活性影響，表現較差。針對遠端及淋巴結轉移方面，^{18}F-FDG PET/CT 表現出極高的敏感度與準確性。研究顯示 ^{18}F-FDG PET/CT 在局部和遠處淋巴結轉移以及隨後的治療判定中具有價值。

^{18}F-FDG PET/CT 提供了癌症病灶的代謝資訊，可以提供放射線治療的劑量區線圈畫參考。研究顯示利用 ^{18}F-FDG PET/CT 影像優化的放射線治療計畫可以在不提高周邊器官輻射劑量下達到針對腫瘤更好的照射劑量集中效果。

^{18}F-FDG PET/CT 衍生的參數 SUVmax、代謝腫瘤體積 (MTV) 和病灶糖酵解總量 (TLG) 逐漸成爲病患預後指標的可能工具。明智的使用 ^{18}F-FDG PET/CT 有助於簡化和提供子宮頸癌患者的臨床處置判斷並優化管理。

關鍵詞：正子造影、子宮頸癌、PET/CT

接受日期：2020 年 5 月 5 日
通訊作者：柴發順
單位：新光吳火獅紀念醫院正子中心
聯絡方式：台北市士林區文昌路 95 號 新光吳火獅紀念醫院正子造影中心
電子郵件：T005629@ms.skh.org.tw

核醫技學誌 2020;17:1-17

前 言

子宮頸癌是台灣地區常見的婦女癌症，依據衛生福利部公告爲 2018 年女性癌症死亡第 7 位 [1]，是全球女性第四大常見癌症，死亡率第四高 [2]。根據美國癌症協會的統計，2017 年有 12,280 例新診斷和 4,210 例死亡歸因於子宮頸癌 [3]。子宮頸癌的發生率在各個國家 / 地區之間差異很大，世界年齡標準化率在每 10 萬名有 1 例至 50 例之間 [4]。在全世界，子宮頸癌是第四大最常見的癌症原因，每年的疾病發生率約爲 569,847 例，死亡 311,365 人 [5]。雖然人類乳突病毒 (HPV) 疫苗接種大大降低發達國家子宮頸癌的發病率和死亡率，但子宮頸癌仍然是全球婦女健康的主要威脅 [3, 6, 7]。

本篇研究的目的在於介紹子宮頸癌並概括敘述 ^{18}F-FDG PET/CT 在子宮頸癌臨床診斷及相關應用價值。

子宮頸癌簡介

子宮頸癌爲女性常見之惡性腫瘤。其中最常見的惡性組織學類型是鱗狀細胞癌 (squamous cell carcinoma)，約佔病例的 80-85%。其餘約 15–20% 的病例是腺癌 (adenocarcinoma) 和腺鱗癌 (adenosquamous carcinoma) [8, 9]。腺癌和腺鱗癌的發病率在許多地區都在增加，這些腫瘤的預後比鱗狀細胞癌差 [10, 11]。

子宮頸癌主要起源於鱗狀小柱交界處 (squamocolumnar junction)，是原位浸潤癌。從病理學上可分爲：

(a) 浸潤前子宮頸癌，也稱爲子宮頸上皮內瘤變 (Cervical Intraepithelial Neoplasia, CIN)
(b) 輕度不典型增生 (CIN I)
(c) 中度不典型增生 (CIN II)
(d) 原位癌的嚴重不典型增生 (CIN III)

儘管並非所有鱗狀上皮內病變都會發展爲癌症，但這些病變被認爲是癌前病變，因此需要評估和積極處置。HPV 類型 16、18、31、33、35、39、45、51、52、56、58、59 和 68 與 CIN 和浸潤性癌症密切相關 [12]。持續感染一種或多種上述致癌類型被認爲是子宮頸腫瘤的必要原因。幾乎所有罹患子宮頸癌的女性都感染了致癌的 HPV 型，HPV 16 和 18 是全世界子宮頸癌中發現的主要病毒基因型，而其他致癌類型 (31、35、45、52 和 58 型) 感染的程度相對較小 [13, 14]。

與子宮頸癌發展相關的其他因素包括早期性行爲、大量的性伴侶、尖銳濕疣病史和吸煙。另外，接受免疫抑製劑的婦女和 HIV 病毒呈陽性的婦女的風險也較高 [11]。

子宮頸癌在早期通常是無症狀的 [15, 16]。年輕患者的性交後出血可能是子宮頸癌的特定症狀，月經間期和絕經後出血是常見和非特異性的症狀，可能表明存在惡性腫瘤 [17]。子宮頸癌病情較嚴重的患者可能會發生血源性擴散。一旦腫瘤開始生長，子宮頸癌會通過基質直接侵入子宮內膜和鄰近結構 (包括陰道、子宮旁膜、膀胱、輸尿管、直腸和子宮頸旁組織) 而擴散，並可以通過淋巴管擴散到骨盆，主動脈旁和鎖骨上的淋巴結。在疾病的任何階段都可能發生血源性擴散到遠處的器官 [18, 19]。一旦被診斷爲子宮頸惡性腫瘤，醫學影像就起著重要作用，因爲其預後受到表現癌症分期，組織學等級，淋巴結狀態等的影響 [20]。

子宮頸癌的分期系統

除了常見的美國癌症聯合委員會 (American Joint Committee on Cancer) 的 TNM 分期系統，另一廣泛被使用的分期系統爲國際婦產科聯合會 (International Federation of Gynecology and Obstetrics, FIGO) 的 FIGO 系統 [21]。之前的 FIGO 系統主要是使用臨床檢查，胸部 X 線照片，靜脈腎盂造影，膀胱鏡檢查和直腸鏡檢查的臨床分期程序 [22, 23]。最近 FIGO 修改了他們的子宮頸癌分期，以便在分配階段時包括影像學和病理學結果 [21]。關鍵的變化是將淋巴結轉移納入分期系統，因爲這對治療和預後有重大影響。FIGO 的分期可參考表 1 和表 2。

常見的美國癌症聯合委員會 (American Joint Committee on Cancer, AJCC) 的 TNM 分期系統是針對惡性腫瘤之不同情況分類，綜合了腫瘤 (T)、淋巴結 (N) 及遠端轉移 (M) 的結果區分不同分期 [24]。子宮頸癌的 TNM 分期可參考表 3、4、5。

這種新的 FIGO 分期系統在美國 SEER 回顧性研究小組中得到了驗證，該研究回顧了 8,909 例 IB 期疾病患者和 11,733 例 III 期患者的因果生存率，並確定了 IB 期和 III 期的不同特徵和生存結果 [25]。與 IB1 期相比，IB2 期子宮頸癌死亡風險幾乎增加了兩倍，調整後的危險 比 (adjusted hazard ratio) 爲 1.98 (95% CI 1.62-2.41)。有趣的是，IIIC1 期婦女的骨盆腔淋巴結轉移具有多種多樣的生存結果，因爲 IIIC1 期 (骨盆腔淋巴結病) 婦女的癌症特異性生存率 (cancer specific survival) 高於 IIIA 至 IIIB 期婦女，IIIA、IIIB、IIIC1 期的 5 年生存率 (5-year survival rates) 分別爲 46%、42.6% 和 62.1%。但是根據 T 分期，IIIC1 期人群的生存率有所不同，5 年生存率：T1 爲 74.8%，T2 爲 58.7%，T3 爲 39.3%。這證明了 IIIC1 期的局限性，該局限性不能解釋存在骨盆腔淋巴結轉移時原發腫瘤內的不均勻性。目前尚無關於 IIIC1 期組淋巴結轉移程度的信息，即體積與鏡檢的相關性，以及關於是否存在主動脈旁淋巴結轉移 (IIIC2 期) 的資料。

子宮頸癌的預後受局部疾病程度的影響，局部疾病的程度取決於腫瘤的大小、深度和腫瘤的浸潤程度、子宮旁的浸潤、骨盆側壁擴展、淋巴結侵犯以及遠處轉移的存在。而腫瘤分級、組織學亞型、患者年齡、腫瘤內充氧、腫瘤血管充盈以及是否存在 HPV 感染是其他影響預後的因素。儘管先前版本的 FIGO 分期主要利用臨床檢查在不易獲得影像的環境中提供統一的分期，但新的 FIGO 分期越來越重視影像學的作用。影像學對於浸潤性器官判定，局部晚期和轉移性疾病的準確分期以及在復發期間進行直接治療很重要。子宮頸癌的分期對於決定治療方法採用手術或放療化療至關重要。外科相關研究的數據表明，一般檢查對疾病的眞實大小和程度的估計能力有限。使用 FIGO 分類，臨床分期將嚴重低估疾病狀態。此外，臨床分期還存在觀察者之間的差異，無法提供明確的淋巴結評估，並且可能完全錯過了子宮旁的侵犯。文獻顯示臨床和手術分期存在明顯差異，範圍從早期疾病 (IIA 期) 的約 25% 到晚期腫瘤 (IIB 期) 的 65-90% [26]。所有這些因素都可能對臨床上被認爲是早期疾病的患者的治療計劃產生重大影響。

表 1：FIGO 子宮頸癌分期 2018

I			癌症嚴格限於子宮頸 (不考慮子宮體的延伸)
			僅可通過顯微鏡診斷的浸潤癌，最大浸潤深度 < 5 mm
	IA	IA1	測得的基質浸潤深度 < 3 mm
		IA2	測得的基質浸潤深度≧ 3 mm 但 < 5 mm
			浸潤癌，浸潤深度最深爲 5 mm (大於 IA 期，病變限於子宮頸）
	IB	IB1	浸潤性癌，間質浸潤深度 5 mm，最大尺寸 < 2 cm
		IB2	浸潤癌最大尺寸≧ 2 cm 和 < 4 cm
		IB3	浸潤癌最大尺寸≧ 4 cm
II			癌侵犯子宮外，但未延伸到陰道下三分之一或骨盆壁
			侵犯僅限於陰道上三分之二而無子宮旁膜侵犯
	IIA	IIA1	浸潤癌最大尺寸 < 4 cm
		IIA2	浸潤癌最大尺寸≧ 4 cm
	IIB		有子宮旁肌侵犯但未到達骨盆壁
III			侵犯陰道下三分之一 / 或延伸至骨盆壁 / 或引起腎積水或腎功能不全 / 或侵犯骨盆或主動脈旁淋巴結
	IIIA		侵犯陰道下部三分之一，未延伸至骨盆壁
	IIIB		延伸至骨盆壁 / 或腎積水 / 或腎功能不全 (除非是由於其他原因引起的)
	IIIC		骨盆腔 / 或主動脈旁淋巴結侵犯，與腫瘤大小和程度無關
		IIIC1	僅骨盆腔淋巴結轉移
		IIIC2	主動脈旁淋巴結轉移
IV			癌已經擴展到了眞正的骨盆之外，或者侵犯膀胱或直腸的粘膜 (切片取樣證實)
	IVA		擴散到鄰近的骨盆器官
	IVB		擴散到遠距的器官

表 2：FIGO 子宮頸癌分期系統的變化

分期	2014 FIGO 系統	2018 FIGO 系統
Stage IB1	腫瘤大小 < 4 cm	腫瘤大小 < 4 cm
Stage IB2	腫瘤大小 > 4 cm	腫瘤大小≧ 2 cm 和 < 4 cm
Stage IB3	n/a	腫瘤大小≧ 4 cm
Stage IIIC1	n/a	僅骨盆腔淋巴結轉移
Stage IIIC2	n/a	主動脈旁淋巴結轉移

表 3：腫瘤 (T) 分期與 FIGO 對照表

T 分期	FIGO 分期	判斷標準
TX		無法評估原發性腫瘤
TO		無原發腫瘤的證據
T1	I	癌症嚴格限於子宮頸 (不考慮子宮體的延伸)
T1a	IA	僅可通過顯微鏡診斷的浸潤癌。從上皮基部測得的最大基質間質浸潤深度爲 5 mm，水平擴散範圍爲 7 mm 或更小。血管、靜脈或淋巴管侵犯不影響分期。
T1a1	IA1	測得的基質浸潤深度爲 3 mm 或更小，水平擴散小於 7 mm
T1a2	IA2	測得的基質浸潤深度介於 3 mm 至 5.0 mm，水平擴散小於 7 mm
T1b	IB	可見的病變限於子宮頸或大於 T1a / IA2 的微觀病變。包括所有肉眼可見的病變和淺表浸潤的病變。
T1b1	IB1	臨床可見病灶最大尺寸爲 4 cm 或更小
T1b2	IB2	臨床可見病變最大尺寸超過 4 cm
T2	II	子宮頸癌侵犯子宮，但未侵犯骨盆壁或陰道下部
T2a	IIA	腫瘤無子宮旁膜浸潤
T2a1	IIA1	臨床可見病變最大尺寸爲 4.0 cm 或更小
T2a2	IIA2	臨床可見病變最大尺寸超過 4.0 cm
T2b	IIB	腫瘤伴隨子宮旁浸潤
T3	III	腫瘤延伸至骨盆側壁 / 或侵犯陰道下三分之一 / 或引起腎積水或腎功能不全
T3a	IIIA	腫瘤侵犯陰道下三分之一，但未延伸至骨盆壁
T3b	IIIB	腫瘤延伸到骨盆壁和 / 或引起腎積水或腎功能不全
T4	IVA	腫瘤侵犯膀胱或直腸粘膜和 / 或延伸超過眞正的骨盆 (腫大水腫不足以將腫瘤分類爲 T4)

表 4：局部淋巴結 (N) 分期

N 分期	判斷標準
NX	無法評估局部淋巴結
N0	無局部淋巴結轉移
N1	局部淋巴結轉移

表 5：遠端轉移 (M) 分期

M 分期	判斷標準
M0	無遠端轉移
M1	遠處轉移 (包括腹膜擴散、鎖骨上、縱隔或腹主動脈旁淋巴結、肺、肝或骨骼侵犯)

CT 與 MRI

在早期研究中，CT 和 MRI 在子宮頸癌分期中的使用，改善了子宮頸癌的臨床分期 [27]。研究表明，MRI 在檢測大於 1 cm 的惡性腫瘤中的準確性爲 85-90% [28]。MRI 可用於對患者進行手術或者放療、化療的分界。MRI 檢測子宮頸癌的子宮旁局部侵犯的敏感度在 75% 至 100% 之間。特異性範圍從 46% 到 86%，陰性預測值很高，爲 94-100%。陽性預測值明顯較低，範圍從 28% 到 77%。MRI 在子宮頸癌分期中的總體準確性約爲 90%。在檢測子宮頸癌的淋巴結轉移方面，MRI 的準確性爲 86% [20, 27, 29-32]。CT 提供了有關子宮頸大小，輸尿管阻塞和遠處轉移的有用信息，但由於軟組織解析度有限，在檢測局部腫瘤範圍中僅扮演次要角色 [33]。CT 對子宮旁浸潤的評估敏感度爲 55%，特異性約爲 74%，但陽性預測值爲 32%，陰性預測值爲 67% [26]。CT 對子宮頸癌分期的準確度爲 65%，對子宮頸癌的淋巴結侵犯的準確度爲 86% [20, 26]。這些 CT 和 MRI 均未描述淋巴結的浸潤。因此在轉移性淋巴結擴散的術前評估中，兩種方式均受到限制。

在子宮頸癌初期階段 MRI 良好的軟組織解析度可準確評估腫瘤體積，腫瘤大小和子宮旁膜浸潤程度。擴散加權成像 (Diffusion Weighted Imaging, DWI) 有助於檢測標準波序中可能看不到的較小病變 [34]。MRI 對子宮內膜的浸潤具有很高的敏感度和特異性分別爲 80% 和 91% [35]。2007 年 156 名女性的實驗中，針對 IIB 分期以上的腫瘤 MRI 的平均敏感度爲 47% (40% 0-57%) 而 CT 的平均敏感度爲 28% (14%-38%)，CT 明顯敏感度較低。CT 的平均特異性 90% (84-100%)，MRI 的平均特異性 79% (77-80%)，另外在腫瘤可視化和子宮旁膜浸潤的檢測方面，MR 成像顯著優於 CT [36]。

PET/CT 子宮頸癌分期應用

子宮頸癌的適當治療取決於準確的分期，以幫助確定進行手術還是非手術治療方式。依照前段文章中對於 FIGO 分期系統的介紹，子宮頸癌初期主要是針對腫瘤體積大小和侵犯程度的分期。^{18}F-FDG PET/CT 是一種非侵入性影像檢查，在許多臨床癌症的診療中是一種有價值的醫學影像檢查 [37-39]。^{18}F-FDG PET/CT 可做爲子宮頸癌癌症分期和再分期以及評估在患者治療中對治療反應的基本方式 [40]，可提供有關腫瘤，淋巴結和轉移的葡萄糖代謝的功能數據。子宮頸癌屬於 FDG 高度活性上升性 (highly FDG avoid) 的腫瘤，FDG 在正常子宮頸中的活性吸收並不明顯高於周圍背景組織的活性吸收 [33]。由於子宮解剖位置上極爲靠近膀胱，FDG 是藉由尿液排出體外，所以膀胱中的高活度累積往往和初期子宮頸癌的 FDG 活性累積相互干擾。由於 PET 的空間解析度有限和部分體積效應 (partial volume effect) 影響，無法準確地顯示子宮旁局部擴散或是陰道侵犯，PET/CT 對早期子宮頸癌的篩查效率較低。

^{18}F-FDG PET/CT 可判定腫瘤向子宮腔內或向下陰道套囊擴展情況下浸潤性腫瘤的邊緣，但可能會漏掉微小轉移病灶，導致僞陰性結果 [41, 42]。^{18}F-FDG PET/CT 在原發性子宮頸病變的表徵或分期中作用較爲有限。Pandharipande 等人的研究報告，PET/CT 在評估局部疾病範圍方面與 MRI 有必不可少的互補作用 [43]。

淋巴結的偵測

淋巴結分期會影響預後和治療計劃，是否存在淋巴結轉移是子宮頸癌預後和治療計劃的最重要決定因素之一 [44]。許多研究評估了 ^{18}F-FDG PET/CT 在評估早期和晚期子宮頸癌中的敏感度和特異性。對於處於晚期 (≥ IB2) 的疾病患者，常有骨盆擴散，包括主動脈旁淋巴結 (paraaortic lymph node, PALN) 侵犯。FDG PET/CT 對淋巴結分期有效，尤其是局部晚期子宮頸癌 (locally advanced cervical carcinoma, LACC)。

Magné 的研究顯示，PET/CT 在局部 CT 陰性的局部晚期子宮頸癌的淋巴結分期中是一種有效的影像檢查技術，可能導致部分患者的治療計劃發生實質性變化 [45]。Grigsby 等，比較了 101 例子宮頸癌患者的 CT 淋巴結分期和全身 ^{18}F-FDG PET/CT 的結果，CT 顯示 101 例患者中 20 例 (20%) 的骨盆腔淋巴結異常增大，而 7 例 (7%) 的主動脈旁淋巴結異常增大。PET 在骨盆腔淋巴結中有 67 例 (67%)，主動脈旁淋巴結中有 21 例 (21%) 和鎖骨上淋巴結中有 8 例 (8%) 異常 FDG 攝取 [46]。

CT 和 MRI 對於淋巴結的診斷主要依賴形態學變化，例如：淋巴結大小。腫瘤中央壞死以及淋巴結邊緣不清，將導致單獨使用尺寸標準作爲淋巴結轉移的標誌是極具欺騙性的 [28, 47]。Hricak 等人試驗中，MRI 和 CT 診斷淋巴結狀態的敏感度較低 (MRI：37% 和 CT：31%) [27]。Wright 等，對臨床上有 ^{18}F-FDG PET/CT 掃描的 IA–IIA

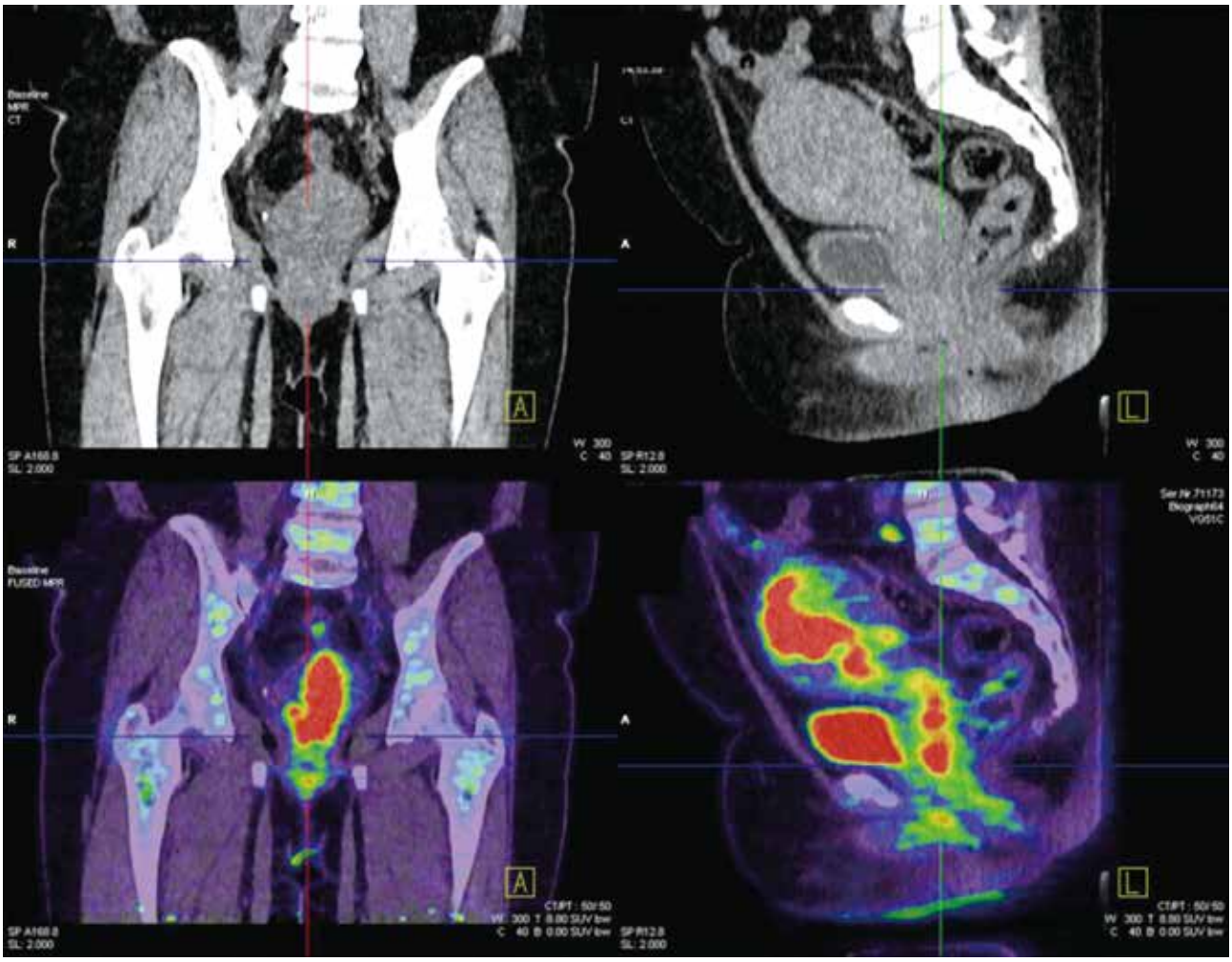

圖 1：^{18}F-FDG PET/CT 掃描發現子宮頸癌侵犯子宮頸、陰道及子宮本體

期患者進行評估，並報告其對淋巴結轉移的敏感度和特異性分別爲 75% 和 90% [48]。Loft 等。用 ^{18}F-FDG PET/CT 前瞻性評估了 120 例 IB 期或以上子宮頸癌患者，並發現 ^{18}F-FDG PET/CT 在這些患者的淋巴結評估中非常有效，骨盆腔淋巴結的敏感度和特異性分別爲 76% 和 96%。對於主動脈旁淋巴結 (PALN) 敏感度和特異性分別爲 100% 和 94% [49]。Rose 等人在研究 PET 在子宮頸癌中的作用的一項初步研究中，將 ^{18}F-FDG PET/CT 檢查結果與 32 例 IIB 至 IVA 子宮頸癌患者淋巴結轉移的手術分期進行了比較。他們發現對骨盆腔淋巴結清掃術的患者在偵測主動脈旁淋巴結轉移中，PET 掃描的敏感性爲 75%，特異性爲 92%，陽性預測值爲 75%，陰性預測值爲 92% [50]。與 CT 和 MRI 相比，PET 在評估淋巴結侵犯方面相當優越。

然而 ^{18}F-FDG PET/CT 在可由外科手術治療的早期子宮頸癌分期中作用是有限的，因爲此階段的淋巴結病變機率低，並且通常是微小轉移病灶。Signorelli 對 159 例子宮切除術和骨盆腔淋巴結切除術前 ^{18}F-FDG PET/CT 影像檢查進行的研究表明，對於早期子宮頸癌 (IB1, IIA 期) ^{18}F-FDG PET/CT 對患者淋巴結轉移的總體敏感度 32.1%，特異性 96.9%，陽性預測值 69.2% 和陰性預測值分別爲 87%，值得注意的是，大多數淋巴結轉移是微轉移，61 個轉移結節中有 34 個轉移結節 < 5 mm。由於 ^{18}F-FDG PET/CT 空間解析度有限，這些小於 5 mm 的微小轉移灶無法檢測到 [51]。

遠端轉移的評估

^{18}F-FDG PET/CT 掃描範圍大，能提供骨盆腔外甚至包含鎖骨上淋巴結，縱隔淋巴結、肺、骨、腹膜、網膜、腎上腺和肝臟等重要器官的診斷資訊來對子宮頸癌的轉移分期 [45]。Wong 等回顧性研究，對 41 例患者進行的總共 61 項 FDG-PET 研究。對子宮頸癌的初始分期，進行了 9 件 FDG-PET 檢查，並在治療後對 35 例不同的患者進行了 52 次 PET 掃描作爲再分期研究。對於子宮頸癌的初始分期實驗中，全部 9 件 ^{18}F-FDG PET 檢查中均確定了局部原發性疾病，PET 將具有局部疾病的 4 名患者與追蹤中有遠處轉移的 5 名患者以 100% 的準確度區分開來。對於子宮頸癌再分期實驗中，PET 對局部復發的評估敏感度爲 82%，特異性爲 97%，準確度爲 92%。評估這些患者的遠處轉移的實驗中，PET 評估遠處病灶的敏感度爲 100%，特異性爲 90%，準確性爲 94% [52]。2018 年一個多中心試驗中回顧了 ^{18}F-FDG PET/CT 偵測遠處轉移情況，28 個地點共納入 153 例子宮頸癌患者和 203 例子宮內膜癌患者，子宮頸癌的遠處轉移率爲 13.7% (21/153)，子宮內膜癌爲 11.8% (24/203)。中心判讀者 (central reader) ^{18}F-FDG PET/CT 檢查在子宮頸癌轉移的特異性 97.7%，陽性預測值和陰性預測值分別爲 79.3% 和 93.1% [53]。研究表明，^{18}F-FDG PET/CT 是子宮頸癌的初始分期和再分期的準確方法。

病人預後評估

標準化攝取值 (standardized uptake value, SUV) 是放射性追蹤劑攝取的一種半定量測量方法，SUV 代表組織活性濃度與特定時間和患者體重的注射劑量的關係，可

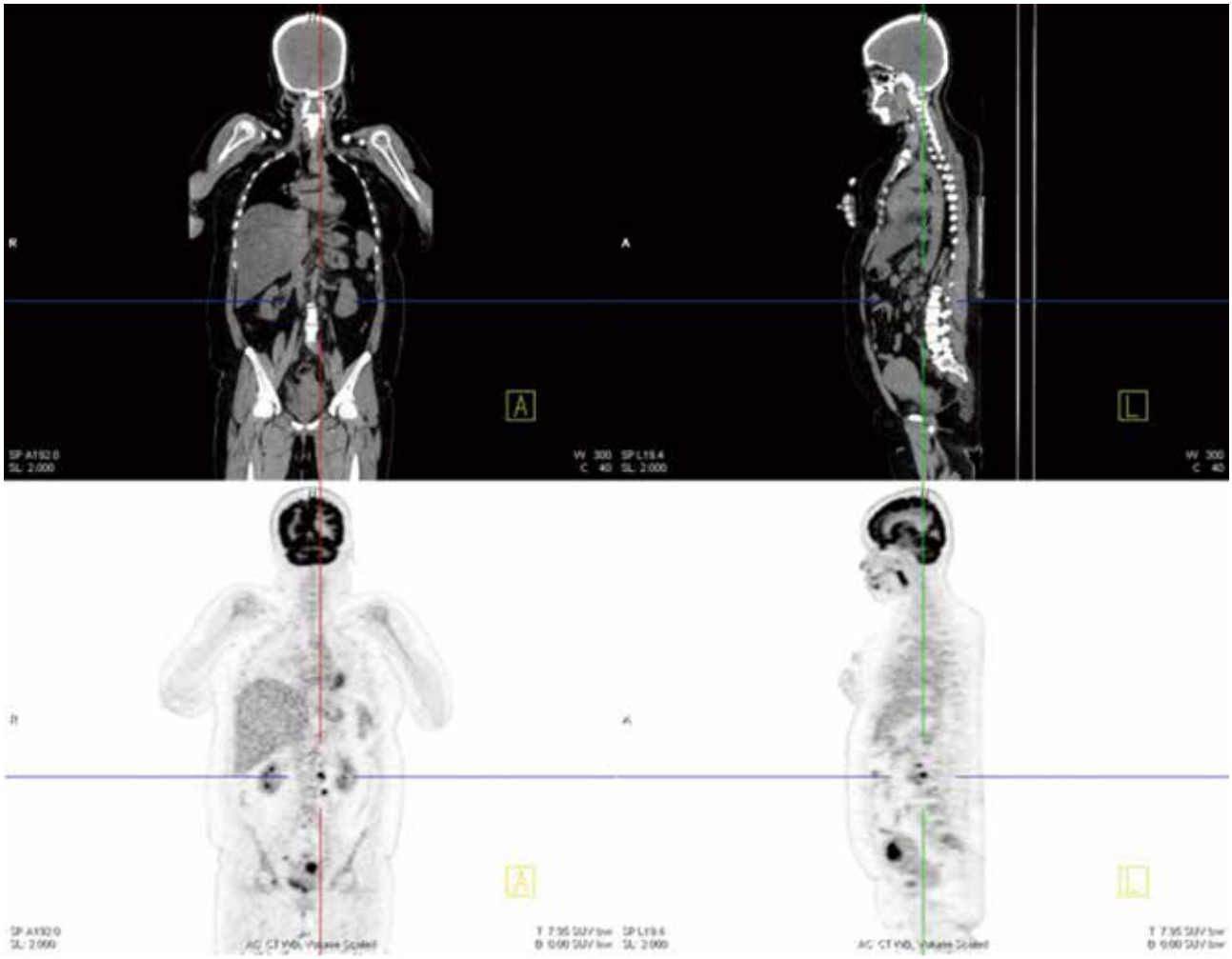

圖 2：^{18}F-FDG PET/CT 發現子宮頸癌遠端淋巴結轉移

用於初步分期和後續反應評估。可以使用標準化攝取值 SUV 進行評估，也可以通過追蹤檢查中 SUV 的下降百分比來評估反應。可以使用 ^{18}F-FDG PET/CT 對腫瘤進行視覺定性和定量分析，目標腫瘤中的最大標準化攝取值 (SUVmax) 反映了腫瘤葡萄糖代謝的程度 [54]。較高的 SUV 與低分化的腫瘤類型有關，鱗狀細胞癌和低分化腫瘤的 SUV 明顯高於非鱗狀細胞癌 [55]。^{18}F-FDG 攝取的程度與腫瘤增殖率相關，反映了腫瘤的侵襲性。Lee 等人還報導了 44 例未經病理組織學確認的 FIGO IB-IIA 期浸潤性子宮頸癌的未經治療患者的 SUV 中位值最高爲 12.3。IB1 期的平均 SUVmax 爲 9.5±6.2 (SD)，IB2 期的平均 SUVmax 爲 17.0±9.5，IIA 期的平均 SUVmax 爲 15.1±6.4，各組之間存在顯著差異 [56]。Yilmaz 等人收集了 43 位子宮頸癌患者，開始治療前接受了 FDG PET/CT 分期，根據原發腫瘤 SUVmax 的中位數將患者分爲低 SUV 組和高 SUV 組。研究發現，子宮頸癌患者淋巴結轉移的可能性隨著原發腫瘤 SUVmax 的增加而增加 [57]。研究表明，原發腫瘤的 SUVmax 可以預測淋巴結轉移的可能性。Kidd 等人研究發現，對於子宮頸癌 FDG PET 的 SUV 可以預測疾病的預後。實驗針對 287 名 IA2-IVB 期患者進行回顧性研究，根據 SUVmax 建立了三個組，其中 SUVmax ≧ 5.2 的 5 年總生存率爲 95%，SUVmax 在 5.2 和 13.3 之間的 5 年總生存率 70%，而 SUVmax > 13.3 的 5 年總生存率爲 44%。在組織學，淋巴結狀態，腫瘤體積和腫瘤 SUVmax 的多變量分析中，SUVmax 是唯一重要的獨立預測因子 [58]。

Onal 等人的進一步研究，在 149 名患者中，與癌症患者或癌症部分緩解患者相比，達到癌症完全緩解患者的腫瘤 SUVmax 明顯低得多，癌症完全緩解患者的 SUVmax 爲 15.6 而部分緩解患者 SUVmax 爲 28.0。骨盆腔淋巴結 SUVmax ≧ 7.5 的患者的原發腫瘤 SUVmax 明顯更高，骨盆腔淋巴結更大，主動脈旁淋巴結轉移率更高，且治療後完全緩解率更低。SUVmax 小於 7.5 患者的總生存率 (Overall survival, OS) 和無病生存率 (disease-free survival, DFS) 顯著更高。在多變量分析中，骨盆淋巴結 SUV 和治療後代謝反應是所有患者總生存率 (OS) 和無病生存率 (DFS) 的重要預後因素 [59]。Ramlov 研究中分析了 SUVmax 與治療後結節控制之間的關係，發現在復發結節中 SUVmax 明顯更高 (p = 0.02)，與結節的大小或體積相比，高結節 SUVmax 是影響結節治療成敗更爲重要的負面預後因素 [60]。Sharma 等發現 FDG 攝取可預測復發子宮頸癌的放射治療後臨床預後，SUVmax 大於 5.8 的患者的 1 年無進展生存率 (1-year progression-free survival rate) 爲 28%，而 SUVmax 小於 5.8 的患者爲 42% (p = 0.01) [61]。Lima 等人針對基於 PET 參數，包括 SUVmax, SUVmean，代謝腫瘤體積 (metabolic tumor volume, MTV) 和 TLG 以及臨床參數，包括年齡、病理學、FIGO 分期和淋巴結轉移等，作爲預測對治療反應的因素的可能作用，評估了放療化療後 3 個月 FDG PET/CT 的預後價值，該研究使用 SUVmax 的變化來指定反應者和非反應者結果表明，根據歐洲癌症研究和治療組織 EORTC 的標準，FDG PET/CT 反應可以可靠地預測生存率，治療前的代謝腫瘤體積 (MTV) 和病灶糖酵解總量 (TLG) 以及淋巴結轉移是對治療反應的預測指標。代謝腫瘤體積 (MTV) 是反應的最佳預測指標 [62]。

子宮頸腫瘤內 FDG 代謝異質性可以預測淋巴結侵犯的風險、對治療的反應以及癌症復發的風險。大多數 FDG-avid 骨盆腔淋巴結的最大尺寸和 SUV 是推論預後的指標，可預測子宮頸癌患者的治療反應、骨盆腔復發風險和疾病特異性生存率 [63, 64]。PET 淋巴結吸收陽性患者的疾病特異性生存率顯著低於 PET 淋巴結吸收陰性患者 (P < .001)。根據 PET 檢測到淋巴結侵犯的最遠程度 (無 / 骨盆 / 主動脈旁或鎖骨上侵犯)，將疾病特異性生存率分爲不同的組。依照淋巴結侵犯的最遠程度，疾病復發的危險比也逐漸增加，侵犯骨盆 2.40 (95%, CI1.63-3.52)，侵犯主動脈旁 5.88 (95%, CI3.80-9.09) 和鎖骨上 30.27 (95%, CI 16.56-55.34)。Yoo 等人研究還發現，在單因素和多因素分析中，代謝腫瘤體積 (metabolic tumor volume, MTV) 和病灶糖酵解總量 (total lesion glycolysis, TLG) 是腫瘤復發或進展的重要預測指標，可用於預測復發和無病生存率，2012 年研究中提出代謝腫瘤體積 (MTV) 臨界值 82 cm (P = 0.001)，病灶糖酵解總量 (TLG) 臨界值 7600 (P = 0.005) [65]。

在許多研究報告中，PET 數據的可視化分析分爲三類：完全代謝反應 (complete metabolic response, CMR)，部分代謝反應 (partial metabolic response, PMR) 和進行性疾病 (progressive disease, PD) 可預測生存率。Schwarz 等人的研究報告中治療後病人的 FDG-PET 顯示 65 例患者完全代謝反應 (70%)，部分代謝反應 15 例 (16%) 和進行性疾病 12 例 (13%)。他們的 3 年無進展生存率 (3-

year progression-free survival rates) 分別爲 78%，33% 和 0% (P < .001)；多變量分析表明，根據顯示出進行性疾病的治療後代謝反應，復發的風險比 (hazard ratio, HR) 爲 32.57。部分代謝反應的 HR 爲 6.30。這些比治療前的淋巴結狀態更能預測生存結果 [66]。

其他研究報導，與 PMR / PD 組相比，CMR 組的總生存率 (OS) 明顯更高。Onal 的研究，CMR 患者的四年總生存率 (OS) 66.9%，PMR / PD 患者則爲 12.4% 明顯更高 (p < 0.001) [67]。Beriwal 的研究 CMR 患者中 9.8% 復發，而 5.4% 局部復發，4.5% 遠處復發。三年無病生存率和總生存率分別爲 78.9% 和 88.0% [68]。

優化放射線治療

放射線治療計劃的主要目標是向腫瘤病灶部位提供最大的輻射劑量並最大程度地減少對正常組織的暴露。傳統上，子宮頸癌的放射治療主要採用的是四照野全骨盆放射治療法 (four-field whole- pelvis radiation therapy)。^{18}F-FDG PET/CT 掃描通過顯示這些部位的轉移，將主動脈旁淋巴結 (PALN) 包括在輻射照野中。這些主動脈旁淋巴結 (PLAN) 可以包含在其他前 - 後或前 - 後照野中 [69, 70]。

想要在正常組織不受到過高輻射劑量的情況下增加腫瘤控制可能性的方法，須設法把腫瘤區域所吸收的放射劑量增加，通常是使用強度調製放射療法 (Intensity-Modulated Radiation Therapy, IMRT) 來執行。強度調控放射治療是以數個治療角度，每個角度分割成許多獨立小射束，藉由調節小射束的放射強度，使高劑量區域在三維方向，能依據腫瘤形狀及深度分布，增加傳遞到腫瘤的劑量並減少相鄰正常結構的暴露：如膀胱、直腸和小腸等的劑量。目前許多治療單位使用 ^{18}F-FDG PET/CT 用於 IMRT 的優化參考。Esthappan 等人的研究，先用 ^{18}F-FDG PET/CT 融合影像用於圈畫子宮頸上的代謝腫瘤體積 (MTV)，在主要部位區畫出 SUVmax 的 40%。以 PET/CT 的 CT 影像用於圈畫出從腎血管到內側迴旋動脈加上 0.7 cm 邊緣的骨盆和主動脈副區域輪廓，以創建臨床目標淋巴結體積。臨床目標淋巴結體積再加上 0.7 cm 的裕度得出實際計劃的腫瘤體積 (淋巴結 PTV)。在融合的 PET/CT 影像上確定 PET 陽性淋巴結，以產生 MTV 淋巴結。所有患者還分六次接受共 39 Gy 的高劑量率近接治療。MTV 淋巴結，PTV 淋巴結和 MTV 子宮頸的目標處方劑量分別爲 30、60、50 和 20 Gy，在所有患者中均已達到，所有計劃均滿足目標覆蓋率目標 [71]。

與基於順鉑 (Cisplatin) 的化學療法相結合，外部放射線光束放射療法仍然是局部晚期子宮頸癌患者的標準療法 [45]。幾項研究表明，通過擴大輻射照野和同時配合化學治療的療法可以治療伴隨主動脈旁淋巴結轉移的子宮頸癌患者 [72-74]。^{18}F-FDG PET/CT 對骨盆腔淋巴結的評估並沒有顯著改變局部病灶的治療，然而病理性腹主動脈旁 FDG 的攝取可能會影響治療策略，^{18}F-FDG PET/CT 在 CT 陰性的局部晚期子宮頸癌的淋巴結分期中是一種有效的成像技術，可能導致部分患者的治療計劃發生實質性變化。^{18}F-FDG PET 爲早期評估治療反應和長期追蹤提供了有意義的信息 [45]。骨盆外淋巴結侵犯可能會改變治療方法，尤其是在最初臨床分期時似乎局限於子宮頸的局部疾病的患者。

Belhocine 對 60 名已經證實的子宮頸癌患者進行了 PET 檢查評估，發現在在 22 例患者中有 4 例 (18%) 因爲治療前分期中在 PET 的發現 (2 例患者有骨盆外淋巴結轉移，另 2 例患者有內臟轉移) 導致改變治療方式，採用替代治療。在 3 例患者中，計劃同時進行放療和化療，並在其中 1 例對大主動脈旁淋巴結進行大範圍放射照射 [75]。

Narayan 等人進行了一項研究，以確定是否可以使用 ^{18}F-FDG PET/CT 或 MRI 取代局部晚期子宮頸癌患者的放射治療計劃中的手術探查分期。作者得出的結論是 PET 在描繪骨盆腔和主動脈旁淋巴結轉移方面的 91% 陽性預測價值似乎足以取代淋巴結取樣，無需手術探查即可擴大放射線範圍，MRI 的準確性不足以影響淋巴結分期，從而影響治療 [76]。儘管 MRI 仍然是用於原發初期子宮頸癌分期的最佳影像檢查技術，但是 PET/CT 已被證明是確定淋巴結狀態的高度靈敏的方法。對於早期子宮頸癌患者來說，PET/CT 無法替代骨盆腔淋巴結的手術探查。在晚期子宮頸癌患者中，PET/CT 可以偵測在骨盆內、骨盆外以及在主動脈旁區域的淋巴結轉移。PET/CT 也被認爲是 3D 適應性近接治療 (3D Conformal Brachytherapy) 的有用工具 [77]。Chao 等人進行了一項前瞻性試驗，該試驗包括 47 例在 CT 或 MRI 中發現有腹主動脈旁、腹股溝或鎖骨上淋巴結轉移的子宮頸癌患者。47 例研究患者中有 21 例 (44.7%) FDG PET 或 PET/CT 對患者的治療有積極的臨床效果 (44.7%)，包括：發

現其他可治癒的部位 (n = 8)，降低疾病的分期 (n = 6)，對相關部位進行代謝取樣 (n = 4) 以及將治療策略改爲緩解 (n = 3)[78]。

近接治療 (Brachytherapy) 是一種放射治療技術，主要是透過密封放射性射源放置於腫瘤區域內，使得腫瘤得到高劑量，且周遭正常組織的劑量會很快速的降低。^{18}F-FDG PET 有助於劃定生理腫瘤的體積並改善腫瘤的靶向劑量 [79]。對於使用 ^{18}F-FDG PET/CT 輔助進行近接治療，也可以進行三維治療計劃，並且被認爲比基於二維正交放射線照射的近接治療計劃更準確 [80]。Lin 等人進行了劑量學研究，針對臨床分期爲 IB1、IIB 和 IIIB 的 11 名接受腔內治療的子宮頸癌患者，共進行 31 次腔內近接治療，比較使用 PET 影像的腫瘤體積優化的治療計畫與標準計劃下的腔內近接治療效果，在第一次放射源植入的平均腫瘤大小爲 56 cm^3 (範圍 7–137 cm^3)，期中 / 最後一次放射源植入物的平均腫瘤大小爲 17 cm^3 (範圍 2–38 cm^3)。研究顯示在開始照射後 20 天內生理腫瘤體積平均減少了 50%。有和沒有優化的情況下，第一次放射源的標靶等劑量表面覆蓋率 (target isodose surface) 分別爲 73% 和 68%。有和沒有優化在期中 / 最後放射源植入的目標等劑量表面的覆蓋百分比分別爲 83% 和 70%。在優化計劃下到達目標 A 點的劑量明顯增加，而膀胱和直腸的劑量均無顯著差異 [81]。Malyapa 等人將常規基於 2D 正交放射線照射的子宮頸癌近接治療計劃與基於 ^{18}F-FDG PET 的 3D 近接治療計劃技術進行了比較，發現根據 3D FDG-PET 劑量 - 體積直方圖確定的最大膀胱和直腸劑量高於使用 2D 治療計劃獲得的最大劑量。這項研究不僅表明 3D 治療計劃相對於常規 2D 治療計劃是可行和準確的，而且 3D 技術在保留關鍵結構的同時具有改善子宮頸癌患者等劑量腫瘤覆蓋率的潛力 [82]。

治療效果評估

根據癌症發展的不同階段，子宮頸癌可以通過手術，放射治療和化學治療法進行治療。多項研究表明，^{18}F-FDG PET/CT 在評估治療反應方面具有價值。Grigsby 等人完成了一項回顧性研究，目的在使用 ^{18}F-FDG PET 對治療後的反應做評估，並將反應與患者預後進行比較。在該回顧性研究中，對 152 例子宮頸癌患者進行了回顧。所有患者均在治療前及治療後接受全身 ^{18}F-FDG PET 掃描。患者接受外部照射和腔內近接放射治療，大多數患者每周同時接受順鉑 (Cisplatin) 藥物治療。在治療後 1–12 個月 (平均 3 個月) 進行全身 ^{18}F-FDG PET 掃描。在 114 例患者中治療後的 PET 掃描皆未顯示任何異常的 ^{18}F-FDG 攝取，其 5 年因病特異性生存率 (5-year cause-specific survival) 估計爲 80%。其中有 20 例患者的子宮頸或淋巴結中 (受輻射照熱區域) 持續存在異常的 ^{18}F-FDG 攝取，5 年因病特異性生存率爲 32%。有 18 例患者在新的解剖部位 (未輻射照射區域) 出現 ^{18}F-FDG 攝取異常攝取，且沒有一個在第五年存活。此項研究表明，在子宮頸癌患者的治療後評估中，^{18}F-FDG PET 的發現可預示生存結果 [83]。

復發偵測

子宮頸癌患者約有三分之一會在 2 年內復發疾病。復發定義爲治療的疾病消退後至少 6 個月的癌症發展 [84]。Wong 等人的研究，評估 ^{18}F-FDG PET 在 41 例子宮頸癌患者中偵測局部和遠處疾病的準確性，其中 35 例在治療後進行分期，結果：對於子宮頸癌再分期，評估局部復發方面，^{18}F-FDG PET 的敏感度爲 82%、特異性爲 97%、準確度爲 92%。評估這些患者的遠端轉移病灶方面，PET 的敏感度爲 100%、特異性爲 90%、準確度爲 94%。此研究證明，PET/CT 對局部復發和遠處轉移性疾病具有很高的準確性，對疾病結果具有預後價值，並有助於改變醫療處置管理 [52]。Crivellaro 等人在 89 例早期子宮頸癌患者中，評估子宮頸癌 FDG 攝取的代謝特徵作爲術前分期中對淋巴結轉移和復發的預測作用。對 PET/CT 影像進行分析，並將其與組織學發現相關聯，通過自適應算法計算子宮頸病變的最大和平均標準化攝取值 (SUVmax, SUVmean)，代謝腫瘤體積 (MTV)，病灶糖酵解總量 (TLG)。這些參數與淋巴結轉移及初次治療後復發的相關性。他們發現在 69 名患者中，pN1 患者的代謝腫瘤體積 (MTV) 和病灶糖酵解總量 (TLG) 顯著高於 pN0 患者 ($p = 0.0006$ 和 $p = 0.03$)，原發性腫瘤的代謝腫瘤體積 (MTV) 和病灶糖酵解總量 (TLG) 與淋巴結轉移有關。在系列研究中，治療前的 ^{18}F-FDG PET/CT 結果無法預測小於 4 cm 早期 FIGO 階段 IB1 和 IIA 子宮頸癌的復發病灶，在該組患者中，復發與 SUVmax, SUVmean，代謝腫瘤體積 (MTV) 或病灶糖酵解總量 (TLG) 之間無顯著相關性 [85]。

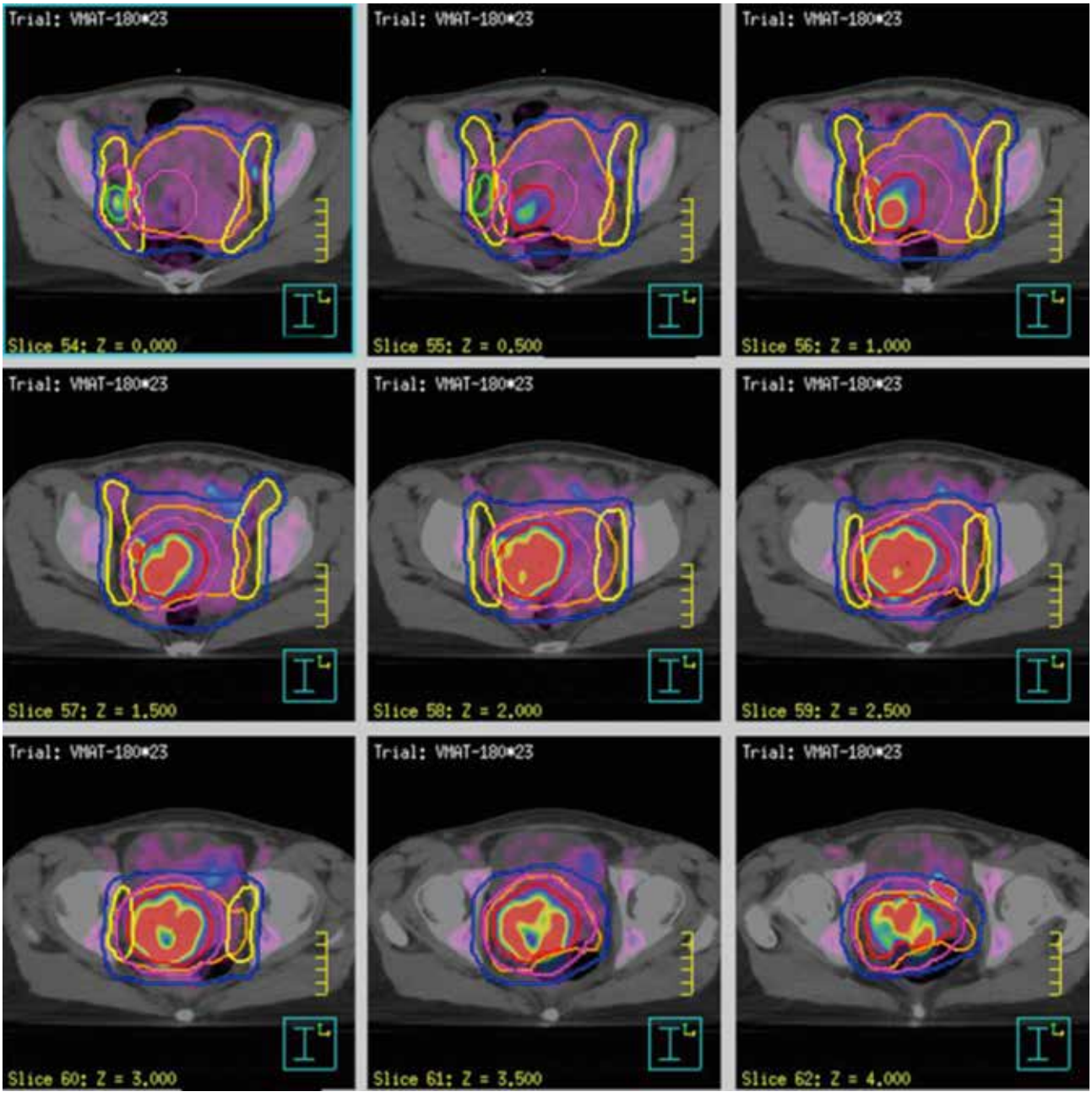

圖 3：以 PET/CT 影像作爲放射治療計畫中圈畫腫瘤照野劑量的參考

缺陷與弱點

^{18}F-FDG PET/CT 是一種影像檢查，可提供有關病灶對於治療法的代謝反應變化的訊息。評估對治療的新陳代謝反應的特徵是這種方式所獨有的。與其他成像方式一樣，^{18}F-FDG PET/CT 也有其局限性，可以通過進一步技術干預來避免。

(a) 骨盆內活性假影：由於 ^{18}F-FDG 主要藉由腎臟清除功能排泄，因此會導致膀胱和輸尿管的大量活性堆積，並可能導致在骨盆區難以判讀。實際操作上可以簡單的操作，例如：在膀胱排空後再掃描骨盆腔或使用留置導尿管以減少活性假影，可以有效地解決此問題。當未停經前婦女卵巢中存在生理性 ^{18}F-FDG 攝取或存在黃體囊

腫時，就會出現判讀困難 [86]，可能無法明確排除潛在的惡性腫瘤。在這種情況下，記錄月經史會有參考幫助。但若是停經後婦女的卵巢有 ^{18}F-FDG 異常攝取，惡性腫瘤的可能性非常高 [87]。

(b) 良性腫瘤或發炎反應中的 ^{18}F-FDG 攝取：某些良性腫瘤可表現出不同的 ^{18}F-FDG 攝取。在這種情況下，SUVmax 值可能並不可靠，因爲變性的平滑肌瘤由於周圍的炎症可能顯示出很高的 ^{18}F-FDG 攝取 [87]。

(c) 治療後發炎反應或骨盆內感染：在手術後早期，由於組織重建和修復程序，骨盆中 ^{18}F-FDG 攝取增加。因此，如果在手術後早期使用 ^{18}F-FDG PET 可能在此類患者中產生僞陽性結果。在這種情況下，^{18}F-FDG PET 雙時間點成像掃描和 ^{18}F-FDG 攝取增減趨勢的觀察可能會有所幫助 [88]。發炎部位預期在延遲影像上顯示 SUVmax 值降低，而惡性部位預期顯示追蹤劑保留或 SUVmax 值進一步增加。但是此項技術並不可靠，也可能是錯誤的。因此，建議在完成外科手術 / 手術後化療或放射治療的患者進行 PET 掃描的間隔爲術後 6-8 週，以避免僞陽性干擾。打算使用 PET 進行治療後反應評估時，還有一種研究觀點主張進行治療前 PET 掃描，此類醫療手段干預前的掃描可估算腫瘤的基線代謝活性，可將其與治療干預後腫瘤代謝狀態進行比較 [89]。

(d) 部分體積效應和極微小病灶：由於技術限制，PET 掃描儀低估了小於 0.7 公分的微小病變中 ^{18}F-FDG 攝取的強度。在這種微觀疾病中，它可能會產生僞陰性結果。在微小肺結節的評估中，這個問題最爲突出 [55]。PET 掃描儀的最新進展，例如新的影像重建運算法、新的追蹤劑、固態檢測器的開發或呼吸門控等新科技或許可以解決並避免這一問題。

結　論

^{18}F-FDG PET/CT 掃描是一種功能強大的影像診斷工具，可在同一次環境中提供功能和解剖學信息。^{18}F-FDG PET/CT 在評估子宮頸癌患者中的作用迅速擴大。^{18}F-FDG PET/CT 被認爲是識別局部和遠處復發性疾病的準確的影像學方法，是非侵入性評估淋巴結狀態的一種檢查選項。研究顯示 PET/CT 在局部和遠處淋巴結轉移以及隨後的治療判定中價值。在放射治療領域，可以提供 IMRT 的代謝腫瘤體積 (MTV) 圈畫參考，從而幫助進行放射治療計劃。^{18}F-FDG PET 衍生的參數 SUVmax、代謝腫瘤體積 (MTV) 和病灶糖酵解總量 (TLG) 逐漸成爲病患預後指標的可能工具。明智的使用 PET/CT 有助於簡化和提供子宮頸癌患者的臨床處置判斷並優化管理。

參考資料

1. Available from: https://www.mohw.gov.tw/cp-16-48057-1.html.
2. Bray, F., et al., *Global cancer statistics 2018: GLOBOCAN estimates of incidence and mortality worldwide for 36 cancers in 185 countries.* CA: a cancer journal for clinicians, 2018. 68(6): p. 394-424.
3. Siegel RL, M. K., Jemal A, *Cancer Statistics, 2017.* CA: A Cancer Journal for Clinicians., 2017. 67(1): p. 7-30.
4. Arbyn, M., et al., *Worldwide burden of cervical cancer in 2008*. Annals of oncology, 2011. 22(12): p. 2675-2686.
5. Bruni L, A. G., Serrano B, Mena M, Gómez D, Muñoz J, Bosch FX, de Sanjosé S., *Human Papillomavirus and Related Diseases in the World. Summary Report* 17 June 2019.
6. Stanley, M., *Human papillomavirus vaccines versus cervical cancer screening*. Clinical oncology, 2008. 20(6): p. 388-394.
7. Plummer, M. and S. Franceschi, *Strategies for HPV prevention*. Virus research, 2002. 89(2): p. 285-293.
8. Eifel, P. J., et al., *Cancer of the cervix, vagina, and vulva, in DeVita, Hellman, and Rosenberg's Cancer: Principles & Practice of Oncology*. 2018, Wolters Kluwer Health Pharma Solutions (Europe) Ltd. p. 1172-1210.
9. Chaturvedi, A. K., et al., *Second cancers after squamous cell carcinoma and adenocarcinoma of the cervix*. Journal of clinical oncology, 2009. 27(6): p. 967.
10. Schorge, J. O., L. M. Knowles, and J. S. Lea, *Adenocarcinoma of the cervix*. Current treatment options in oncology, 2004. 5(2): p. 119-127.
11. Imadome, K., et al., *Subtypes of cervical adenosquamous carcinomas classified by EpCAM expression related to radiosensitivity*. Cancer biology & therapy, 2010. 10(10): p. 1019-1026.
12. Walboomers, J. M., et al., *Human papillomavirus is a*

necessary cause of invasive cervical cancer worldwide. The Journal of pathology, 1999. 189(1): p. 12-19.
13. Koutsky, L. A., et al., *A controlled trial of a human papillomavirus type 16 vaccine*. New England Journal of Medicine, 2002. 347(21): p. 1645-1651.
14. Ling, M., et al., *Preventive and therapeutic vaccines for human papillomavirus-associated cervical cancers*. Journal of biomedical science, 2000. 7(5): p. 341-356.
15. Kumar, V., A. K. Abbas, and J.C. Aster, Robbins basic pathology e-book. 2017: Elsevier Health Sciences.
16. Canavan, T. P. and N. R. Doshi, *Cervical cancer*. American family physician, 2000. 61(5): p. 1369-1376.
17. James, R., M. Cruickshank, and N. Siddiqui, *Management of cervical cancer: summary of SIGN guidelines*. Bmj, 2008. 336(7634): p. 41-43.
18. Kindermann, G. and H.-P. Jabusch, *The spread of squamous cell carcinoma of the uterine cervix into the blood-vessels*. Archiv für Gynäkologie, 1972. 212(1): p. 1-8.
19. Eifel, P., et al., *Cancer of the Female Lower Genital Tract*. 2001: BC Decker.
20. Subak, L. E., et al., *Cervical carcinoma: computed tomography and magnetic resonance imaging for preoperative staging*. Obstetrics & Gynecology, 1995. 86(1): p. 43-50.
21. Bhatla, N., et al., *Cancer of the cervix uteri*. International Journal of Gynecology & Obstetrics, 2018. 143: p. 22-36.
22. Sergio, P., *Staging Classifications and Clinical Practice Guidelines for Gynaecologic Cancers*. Int J Gynecol Obst, 2000. 70: p. 95-121.
23. Benedet, J., et al., *Staging classifications and clinical practice guidelines for gynaecological cancers*. International Journal of Gynecology and Obstetrics, 2000. 70: p. 207-312.
24. Amin, M. B., et al., *AJCC Cancer Staging Manual*. 2018: Springer International Publishing.
25. Matsuo, K., et al., *Validation of the 2018 FIGO cervical cancer staging system*. Gynecologic oncology, 2019. 152(1): p. 87-93.
26. Bipat, S., et al., *Computed tomography and magnetic resonance imaging in staging of uterine cervical carcinoma: a systematic review*. Gynecologic oncology, 2003. 91(1): p. 59-66.
27. Hricak, H., et al., *Role of imaging in pretreatment evaluation of early invasive cervical cancer: results of the intergroup study American College of Radiology Imaging Network 6651–Gynecologic Oncology Group 183*. Journal of clinical oncology, 2005. 23(36): p. 9329-9337.
28. Yang, W. T., et al., *Comparison of dynamic helical CT and dynamic MR imaging in the evaluation of pelvic lymph nodes in cervical carcinoma*. American Journal of Roentgenology, 2000. 175(3): p. 759-766.
29. Hricak, H., et al., *Invasive cervical carcinoma: comparison of MR imaging and surgical findings*. Radiology, 1988. 166(3): p. 623-631.
30. Sheu, M.-H., et al., *Preoperative staging of cervical carcinoma with MR imaging: a reappraisal of diagnostic accuracy and pitfalls*. European radiology, 2001. 11(9): p. 1828-1833.
31. Kim, S. H., et al., *Preoperative staging of uterine cervical carcinoma: comparison of CT and MRI in 99 patients*. Journal of computer assisted tomography, 1993. 17(4): p. 633-640.
32. Chung, H. H., et al., *Can preoperative MRI accurately evaluate nodal and parametrial invasion in early stage cervical cancer?* Japanese journal of clinical oncology, 2007. 37(5): p. 370-375.
33. Follen, M., et al., *Imaging in cervical cancer*. Cancer: Interdisciplinary International Journal of the American Cancer Society, 2003. 98(S9): p. 2028-2038.
34. Khan, S. R., A. G. Rockall, and T. D. Barwick, *Molecular imaging in cervical cancer*. The quarterly journal of nuclear medicine and molecular imaging: official publication of the Italian Association of Nuclear Medicine (AIMN) [and] the International Association of Radiopharmacology (IAR), [and] Section of the Society of... 2016. 60(2): p. 77-92.
35. desouza, N. M., et al., *Cervical cancer: value of an*

endovaginal coil magnetic resonance imaging technique in detecting small volume disease and assessing parametrial extension. Gynecologic oncology, 2006. 102(1): p. 80-85.

36. Hricak, H., et al., *Early invasive cervical cancer: CT and MR imaging in preoperative evaluation – ACRIN/GOG comparative study of diagnostic performance and interobserver variability. Radiology*, 2007. 245(2): p. 491-498.
37. Davison, J. M., et al., *Squamous cell carcinoma of the palatine tonsils: FDG standardized uptake value ratio as a biomarker to differentiate tonsillar carcinoma from physiologic uptake*. Radiology, 2010. 255(2): p. 578-585.
38. Jackson, T., et al., *FDG PET/CT interobserver agreement in head and neck cancer: FDG and CT measurements of the primary tumor site*. Nuclear medicine communications, 2012. 33(3): p. 305-312.
39. Nabi, H. A. and J. M. Zubeldia, *Clinical applications of 18F-FDG in oncology*. Journal of nuclear medicine technology, 2002. 30(1): p. 3-9.
40. Park, W., et al., *The usefulness of MRI and PET imaging for the detection of parametrial involvement and lymph node metastasis in patients with cervical cancer*. Japanese journal of clinical oncology, 2005. 35(5): p. 260-264.
41. Grigsby, P. W., *The contribution of new imaging techniques in staging cervical cancer*. Gynecologic oncology, 2007. 107(1): p. S10-S12.
42. Chou, H.-H., et al., *Low value of [18F]-fluoro-2-deoxy-D-glucose positron emission tomography in primary staging of early-stage cervical cancer before radical hysterectomy*. Journal of clinical oncology, 2006. 24(1): p. 123-128.
43. Pandharipande, P. V., et al., *MRI and PET/CT for triaging stage IB clinically operable cervical cancer to appropriate therapy: decision analysis to assess patient outcomes*. American Journal of Roentgenology, 2009. 192(3): p. 802-814.
44. Stehman, F. B., et al., *Carcinoma of the cervix treated with radiation therapy I. A multi variate analysis of prognostic variables in the gynecologic oncology group*. Cancer, 1991. 67(11): p. 2776-2785.
45. Magné, N., et al., *New trends in the evaluation and treatment of cervix cancer: the role of FDG–PET*. Cancer treatment reviews, 2008. 34(8): p. 671-681.
46. Grigsby, P. W., B. A. Siegel, and F. Dehdashti, *Lymph node staging by positron emission tomography in patients with carcinoma of the cervix*. Journal of Clinical Oncology, 2001. 19(17): p. 3745-3749.
47. Bell, D. J. and H. K. Pannu, *Radiological assessment of gynecologic malignancies*. PET clinics, 2010. 5(4): p. 407-423.
48. Wright, J. D., et al., *Preoperative lymph node staging of early stage cervical carcinoma by [18F] fluoro 2 deoxy D glucose–positron emission tomography*. Cancer: Interdisciplinary International Journal of the American Cancer Society, 2005. 104(11): p. 2484-2491.
49. Loft, A., et al., *The diagnostic value of PET/CT scanning in patients with cervical cancer: a prospective study*. Gynecologic oncology, 2007. 106(1): p. 29-34.
50. Rose, P., et al., *PET for evaluating para-aortic nodal metastasis in locally advanced cervical cancer before surgical staging: a surgicopathologic study*. J Clin Oncol, 1999. 17: p. 41-5.
51. Signorelli, M., et al., *Preoperative staging of cervical cancer: is 18-FDG-PET/CT really effective in patients with early stage disease?* Gynecologic oncology, 2011. 123(2): p. 236-240.
52. Wong, T. Z., E. L. Jones, and R. E. Coleman, *Positron emission tomography with 2-deoxy-2-[18F] fluoro-D-glucose for evaluating local and distant disease in patients with cervical cancer*. Molecular Imaging & Biology, 2004. 6(1): p. 55-62.
53. Gee, M. S., et al., *Identification of distant metastatic disease in uterine cervical and endometrial cancers with FDG PET/CT: analysis from the ACRIN 6671/GOG 0233 multicenter trial*. Radiology, 2018. 287(1): p. 176-184.
54. Lin, L. L., et al., *FDG-PET imaging for the assessment*

of physiologic volume response during radiotherapy in cervix cancer. International Journal of Radiation Oncology* Biology* Physics, 2006. 65(1): p. 177-181.

55. Son, H., et al., *PET/CT evaluation of cervical cancer: spectrum of disease*. Radiographics, 2010. 30(5): p. 1251-1268.
56. Lee, Y.-Y., et al., *The prognostic significance of the SUVmax (maximum standardized uptake value for F-18 fluorodeoxyglucose) of the cervical tumor in PET imaging for early cervical cancer: preliminary results*. Gynecologic oncology, 2009. 115(1): p. 65-68.
57. Yilmaz, M., et al., *FDG PET-CT in cervical cancer: relationship between primary tumor FDG uptake and metastatic potential.* Nuclear medicine communications, 2010. 31(6): p. 526-531.
58. Kidd, E. A., et al., *The standardized uptake value for F18 fluorodeoxyglucose is a sensitive predictive biomarker for cervical cancer treatment response and survival*. Cancer, 2007. 110(8): p. 1738-1744.
59. Onal, C., et al., *Prognostic value of 18F-fluorodeoxyglucose uptake in pelvic lymph nodes in patients with cervical cancer treated with definitive chemoradiotherapy*. Gynecologic oncology, 2015. 137(1): p. 40-46.
60. Ramlov, A., et al., *Impact of radiation dose and standardized uptake value of (18) FDG PET on nodal control in locally advanced cervical cancer*. Acta Oncologica, 2015. 54(9): p. 1567-1573.
61. Sharma, D. N., et al., *Positron emission tomography scan for predicting clinical outcome of patients with recurrent cervical carcinoma following radiation therapy*. Journal of cancer research and therapeutics, 2012. 8(1): p. 23.
62. Lima, G. M., et al., *Prognostic value of posttreatment 18 F-FDG PET/CT and predictors of metabolic response to therapy in patients with locally advanced cervical cancer treated with concomitant chemoradiation therapy: an analysis of intensity-and volume-based PET parameters*. European journal of nuclear medicine and molecular imaging, 2018. 45(12): p. 2139-2146.
63. Kidd, E. A. and P. W. Grigsby, *Intratumoral metabolic heterogeneity of cervical cancer*. Clinical cancer research, 2008. 14(16): p. 5236-5241.
64. Kidd, E. A., et al., *Lymph node staging by positron emission tomography in cervical cancer: relationship to prognosis.* J Clin Oncol, 2010. 28(12): p. 2108-2113.
65. Yoo, J., et al., *ATL*. International Journal of Gynecologic Cancer, 2012. 22(7): p. 1226-1233.
66. Schwarz, J. K., et al., *Association of posttherapy positron emission tomography with tumor response and survival in cervical carcinoma*. Jama, 2007. 298(19): p. 2289-2295.
67. Onal, C., et al., *Treatment outcomes of patients with cervical cancer with complete metabolic responses after definitive chemoradiotherapy*. European journal of nuclear medicine and molecular imaging, 2014. 41(7): p. 1336-1342.
68. Beriwal, S., et al., *Complete metabolic response after definitive radiation therapy for cervical cancer: patterns and factors predicting for recurrence*. Gynecologic oncology, 2012. 127(2): p. 303-306.
69. Bradley, K. A. and D. G. Petereit, *Radiation therapy for gynecologic malignancies*. Hematology/Oncology Clinics, 2006. 20(2): p. 347-361.
70. Millar, L. B. and L. L. Lin, *RADIATION THERAPY FOR GYNECOLOGIC MALIGNANCIES, in Manual Of Gynecologic Oncology.* 2011, World Scientific. p. 37-66.
71. Esthappan, J., et al., *Prospective clinical trial of positron emission tomography/computed tomography image-guided intensity-modulated radiation therapy for cervical carcinoma with positive para-aortic lymph nodes*. International Journal of Radiation Oncology* Biology* Physics, 2008. 72(4): p. 1134-1139.
72. Morris, M., et al., *Pelvic radiation with concurrent chemotherapy compared with pelvic and para-aortic radiation for high-risk cervical cancer*. New England Journal of Medicine, 1999. 340(15): p. 1137-1143.
73. Ansink, A., et al., *Recurrent stage IB cervical carcinoma: evaluation of the effectiveness of routine follow up surveillance.* BJOG: An International Journal of

Obstetrics & Gynaecology, 1996. 103(11): p. 1156-1158.
74. Stryker, J. A. and R. Mortel, *Survival following extended field irradiation in carcinoma of cervix metastatic to para-aortic lymph nodes*. Gynecologic oncology, 2000. 79(3): p. 399-405.
75. Belhocine, T., et al., *Contribution of whole-body 18FDG PET imaging in the management of cervical cancer.* Gynecologic oncology, 2002. 87(1): p. 90-97.
76. Narayan, K., et al., *A comparison of MRI and PET scanning in surgically staged loco-regionally advanced cervical cancer: potential impact on treatment*. International Journal of Gynecologic Cancer, 2001. 11(4): p. 263-271.
77. Haie-Meder, C., R. Mazeron, and N. Magné, *Clinical evidence on PET–CT for radiation therapy planning in cervix and endometrial cancers*. Radiotherapy and Oncology, 2010. 96(3): p. 351-355.
78. Chao, A., et al., *Positron emission tomography in evaluating the feasibility of curative intent in cervical cancer patients with limited distant lymph node metastases*. Gynecologic oncology, 2008. 110(2): p. 172-178.
79. Hillner, B. E., et al., *Relationship between cancer type and impact of PET and PET/CT on intended management: findings of the national oncologic PET registry*. Journal of Nuclear Medicine, 2008. 49(12): p. 1928-1935.
80. Macdonald, D. M., et al., *Combined intensity-modulated radiation therapy and brachytherapy in the treatment of cervical cancer.* International Journal of Radiation Oncology* Biology* Physics, 2008. 71(2): p. 618-624.
81. Lin, L. L., et al., *Adaptive brachytherapy treatment planning for cervical cancer using FDG-PET*. International Journal of Radiation Oncology* Biology* Physics, 2007. 67(1): p. 91-96.
82. Malyapa, R. S., et al., P*hysiologic FDG-PET three-dimensional brachytherapy treatment planning for cervical cancer*. International Journal of Radiation Oncology* Biology* Physics, 2002. 54(4): p. 1140-1146.
83. Grigsby, P. W., et al., *Posttherapy [18F] fluorodeoxyglucose positron emission tomography in carcinoma of the cervix: response and outcome*. Journal of clinical oncology, 2004. 22(11): p. 2167-2171.
84. Heron, C. W., et al., *The value of CT in the diagnosis of recurrent carcinoma of the cervix*. Clinical radiology, 1988. 39(5): p. 496-501.
85. Crivellaro, C., et al., *18F-FDG PET/CT can predict nodal metastases but not recurrence in early stage uterine cervical cancer*. Gynecologic oncology, 2012. 127(1): p. 131-135.
86. Ho, K., et al., *An ovary in luteal phase mimicking common iliac lymph node metastasis from a primary cutaneous peripheral primitive neuroectodermal tumour as revealed by 18-fluoro-2-deoxyglucose positron emission tomography*. The British journal of radiology, 2005. 78(928): p. 343-345.
87. Choudhary, S., et al., *Imaging of ovarian teratomas: appearances and complications*. Journal of medical imaging and radiation oncology, 2009. 53(5): p. 480-488.
88. Blake, M. A., et al., *Pearls and pitfalls in interpretation of abdominal and pelvic PET-CT*. Radiographics, 2006. 26(5): p. 1335-1353.
89. Herrmann, K., et al. *Monitoring response to therapeutic interventions in patients with cancer. in Seminars in nuclear medicine*. 2009. Elsevier.

Clinical Value of ^{18}F-FDG PET/CT in Cervical Cancer

Fa-Shun Tsai*, Tai-Lin Jiang, Lin-Chun Ou, Cheng-Hui Lee

Division of PET Center, Shin Kong Wu Ho-Su Memorial Hospital, Taipei, Taiwan

Abstract

Worldwide, cervical cancer was the fourth most common cancer among women. The purpose of this study is to introduce cervical cancer and outline the clinical value of ^{18}F-FDG PET/CT in the diagnosis and treatment of cervical cancer.

The FIGO (International Federation of Gynecology and Obstetrics) staging system is used most often for cancers of the female reproductive organs, including cervical cancer. Recently, FIGO staging has incorporated lymph node metastasis into the staging system because it has a significant impact on treatment and prognosis. In the early stage of cervical cancer, MRI and CT showed quite good sensitivity and accuracy. ^{18}F-FDG PET/CT performed poorly due to the poor soft tissue resolution and affected by the urine radioactivity. In terms of distal and lymph node metastasis, ^{18}F-FDG PET/CT shows extremely high sensitivity and accuracy. Studies have shown that ^{18}F-FDG PET/CT has great value in local and distant lymph node metastasis and subsequent treatment decisions.

^{18}F-FDG PET/CT provides metabolic information of cancer lesions, and can provide a reference for drawing the dose area of radiation therapy. Studies have shown that radiotherapy plans optimized with ^{18}F-FDG PET/CT images can achieve better radiation dose distribution for tumors without increasing the radiation dose of peripheral organs.

The parameters as SUVmax, MTV and TLG derived from ^{18}F-FDG PET/CT have gradually become possible stratification tools for prognostic indicators of patients. The wise use of ^{18}F-FDG PET/CT helps to simplify and direct patient care, and optimize management of cervical cancer patients.

Key words: PET, PET/CT, ^{18}F-FDG, Cervical cancer

J Nucl Med Tech 2020;17:1-17

Received 2020/5/5
Corresponding author: Fa-Shun Tsai
Division of PET Center, Shin Kong Wu Ho-Su Memorial Hospital, Taipei, Taiwan
Address: No. 95, Wenchang Rd., Shilin Dist., Taipei City 111, Taiwan (R.O.C.) Division of PET Center
E-mail: T005629@ms.skh.org.tw

The Demonstration of the Radiation Shielding Ability of Lead Apron: A Monte Carlo Simulation Experiment

Fa-Shun Tsai*, Tai-Lin Jiang, Lin-Chun Ou, Cheng-Hui Lee

Division of PET Center, Shin Kong Wu Ho-Su Memorial Hospital, Taipei, Taiwan

Abstract:

For reducing radiation exposure, there are three principals: time, distance, and shielding. In traditional radiological departments, shielding by lead aprons is the most common protective practice. The photon energy of the radioisotope used in the nuclear medicine department is much higher than the X-ray energy traditionally used in diagnosis. Therefore, it is questionable whether the lead coat under the same lead equivalent can provide appropriate radiation protection for the staff of the nuclear medicine department. In this study, a Monte Carlo simulation experiment was used to verify and demonstrate the shielding effect of lead clothing with a lead equivalent thickness of 0.5 mm.

Materials and Methods

Using GATE software to simulate 50 keV, 140 keV, 511 keV, 1 MeV single energy photons and X-rays with tube voltage of 80, 100, 120, 140 kVp, irradiating a 30 × 30 × 30 cm water phantom. Simulate the 10^6 photons direct irradiation and irradiated with 0.5 mm thickness lead shielding, respectively. Record the dose per 1 mm thickness of water, the unit is Gray (Gy).

Results

Without lead shielding, the radiation doses for X-rays irradiated with water with a tube voltage of 80, 100, 120, 140 kVp were 6.05×10^{-8}, 6.53×10^{-8}, 6.96×10^{-8}, 7.35×10^{-8} Gy, the doses with 0.5 mm lead plate were 2.47×10^{-9}, 5.11×10^{-9}, 6.10×10^{-9}, 7.09×10^{-9} Gy. The remaining dose with lead plate were 4.08%, 7.81%, 8.76%, and 9.65% of no lead plate was used. Lead plate which had a significant effect on X-ray protection. Under the irradiation of 50 keV, 140 keV, 511 keV and 1 MeV single energy photons, the radiation dose of the water phantom were 6.51×10^{-7}, 1.43×10^{-7}, 5.79×10^{-7}, 1.12×10^{-6} Gy, respectively. The dose of protection using 0.5 mm lead plate were 1.04×10^{-9}, 3.96×10^{-8}, 5.42×10^{-7}, 1.09×10^{-6} Gy. The exposure after using lead protection is 1.59%, 27.76%, 93.54%, 97.25% of no lead plate was used, which performance is not good for 511 keV and 1 MeV photons protection.

Conclusion

The simulation data shows that the lead clothing, commonly used in clinical practice with an equivalent thickness of 0.5 mm, has a very good protective effect on X-ray irradiation of 80, 100, 120, 140 kVp, and the staff of traditional radiation inspection units should indeed wear protection. The photon energy of the radioisotope used by the nuclear medicine department is higher, and the protective effect of lead clothing with a lead equivalent thickness of 0.5 mm is not ideal. For positron imaging 511 keV high-energy photons, the protection of lead plates with a thickness of more than 4 mm is required to achieve 50% of the protection effect. In practice, it is impossible to wear such a thickness of lead coat protection. It should be considered to

Received 2020/7/27
Corresponding author: Fa-Shun Tsai
Division of PET Center, Shin Kong Wu Ho-Su Memorial Hospital, Taipei, Taiwan
Address: No. 95, Wenchang Rd., Shilin Dist., Taipei City 111, Taiwan (R.O.C.)
Division of PET Center
E-mail: T005629@ms.skh.org.tw

optimize the work process to reduce exposure time and sufficient thickness of lead bricks and lead plates should be considered.

Key words: lead apron, Monte Carlo simulation, X-ray, radiation dose, radiation protection

J Nucl Med Tech 2020;17:19-27

There is no doubt that radiation exposure in sufficient amounts can cause harm. There are three general guidelines for controlling exposure to ionizing radiation: minimizing exposure time, maximizing distance from the radiation source and shielding yourself from the radiation source. It also called the "TDS principals": time, distance, and shielding. There are many shielding devices such as caps, lead glasses, thyroid protectors, aprons, radiation reducing gloves, and so on. In traditional radiological departments, shielding by lead aprons is the most common protective practice [1].

X-rays are high-energy photons, which produced by bombarding a metallic anode with electrons. The x-ray spectrum produced by the x-ray tube including the bremsstrahlung radiation and characteristic x-rays. Bremsstrahlung radiation is a continuum with maximal energy at a keV equal to tube voltage. Characteristic x-rays are due to electron ejection events; the hole is filled by another electron, which emits an x-ray at a specific energy. Note that the average energy of the beam is much less than the peak energy; a rule of thumb is that it would be 1/3 of the maximum energy [2]. The average energy of x-rays with tube voltage of 120 kVp is around 40 keV.

Nuclear medicine department uses small amounts of radioactive materials called radiotracers for imaging diagnosis, evaluate or treat a variety of diseases. Radiotracers are molecules labeled with a radioactive isotope. The most common radioisotope used in image diagnosis is technetium-99m (^{99m}Tc), emits readily detectable gamma rays with a photon energy of 140 keV [3]. Positron emission tomography is a branch of nuclear medicine imaging. PET technique uses positron emission isotope labeled radio-tracer for imaging. As the radioisotope undergoes positron emission decay, it emits a positron, an antiparticle of the electron with opposite charge. The emitted positron travels in tissue for a short distance until it decelerates to a point where it can interact with an electron. The encounter annihilates both electron and positron, producing a pair of 511 keV annihilation gamma photons moving in approximately opposite directions [4].

Shielding by lead aprons is the most common protective practice In radiology department. Lead protective garments are standard required protection to anyone being exposed to radiation. Lead aprons and vest garments need to be between 0.35 and 0.5 mm lead equivalent thickness. The garments not only protect the covered organs but also reduce the total body effective dose of exposure as much as 16-fold [5]. The photon energy of the radioisotope used in the nuclear medicine department is considerably higher than that of the X-rays traditionally used in the diagnoses. Is 0.5 mm lead equivalent thickness lead apron still performance well in nuclear medicine department?

In this study, we attempt to use the Monte Carlo simulation program to verify and demonstrate the shielding effect of lead clothing with a lead equivalent thickness of 0.5 mm.

Materials and Methods

The GEANT4 Application for Emission Tomography (GATE) encapsulates the GEANT4 libraries in order to achieve a modular, versatile, scripted simulation toolkit adapted to the field of nuclear medicine. In particular, GATE provides the capability for modeling time-dependent phenomena such as detector movements or source decay kinetics, thus allowing the simulation of time curves under realistic acquisition condition [6, 7]. All of the Monte Carlo simulations were performed using the GATE version 7.2 with GEANT4 version 4.10 in this study. System geometric setting: The Photon source set as "General Particle Source". Source surface distance (SSD) is 5 cm, the beam shape as a 3mm wide pencil beam. The lead plate with 0.5 mm (Pb 0.5 mm) thickness is 1cm above the water phantom.

Each test simulates 10^6 photons of 50, 140, 511, 1000 keV mono-energy photons and 80, 100, 120, 140 kVp tube voltage x-rays irradiating on 30 × 30 × 30 cm water phantom. The x-ray spectrum is generated by SPEKTR 3.0 [8]. The SPEKTR is a computational toolkit witch has been developed to calculate x-ray spectra based on the TASMICS algorithm, updating previous work based on the TASMIP spectral model. The toolkit includes a Matlab function library and improved user interface (UI) along with an optimization algorithm to match calculated beam quality with measurements. The SPEKTR 3.0 setting GUI as illustrated in Figure 1.

The beam hits the water cube surface and deposits a dose under the surface of the water. A "DoseActor" with matrix size 1 × 1 × 300 is attached to the water cube. The volume of the water cube is divided into 300 slices perpendicular to the incident beam. At each slice the deposited energy is computed. This actor recodes 1D dose distribution of the dose deposited and the number of hits in a given volume. The unit of dose deposited is Gray (Gy).

Result

A plot of number of photons per energy interval versus photon energy is referred to as a photon spectrum. The x-ray spectrum incents the water cube with and without lead shielding were showed as Figure 2. The maximum energy in kiloelectron volts (keV) is numerically equal to the voltage difference between the anode and the cathode in kilovolts peak (kVp). You can see that the area under the curve is significantly reduced. The 0.5 mm lead plate as a filter, resulting in selective attenuation of lower energy photons.

In Geant4, when a hit occur, energy is deposited along a step line. We plot the x-ray dose deposition along the depth of the water absorber as Figure 3. The absorbed dose corves with Pb 0.5 mm shielding were significantly lower than these without shielding. Total absorbed dose within the water

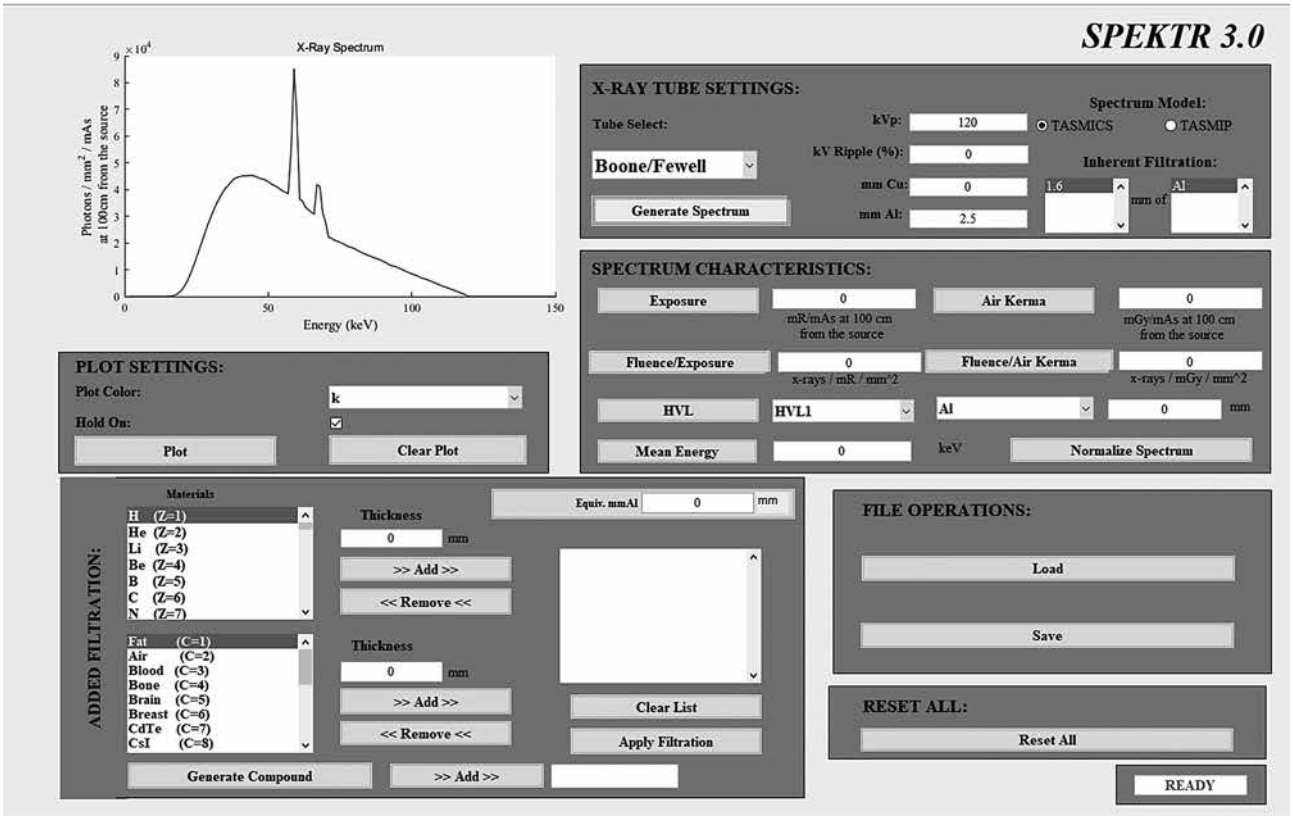

Figure 1. The GUI of the SPEKTR 3.0 software. The GUI allows users to generate x-ray spectra, modify filtration, and calculate beam-quality characteristics.

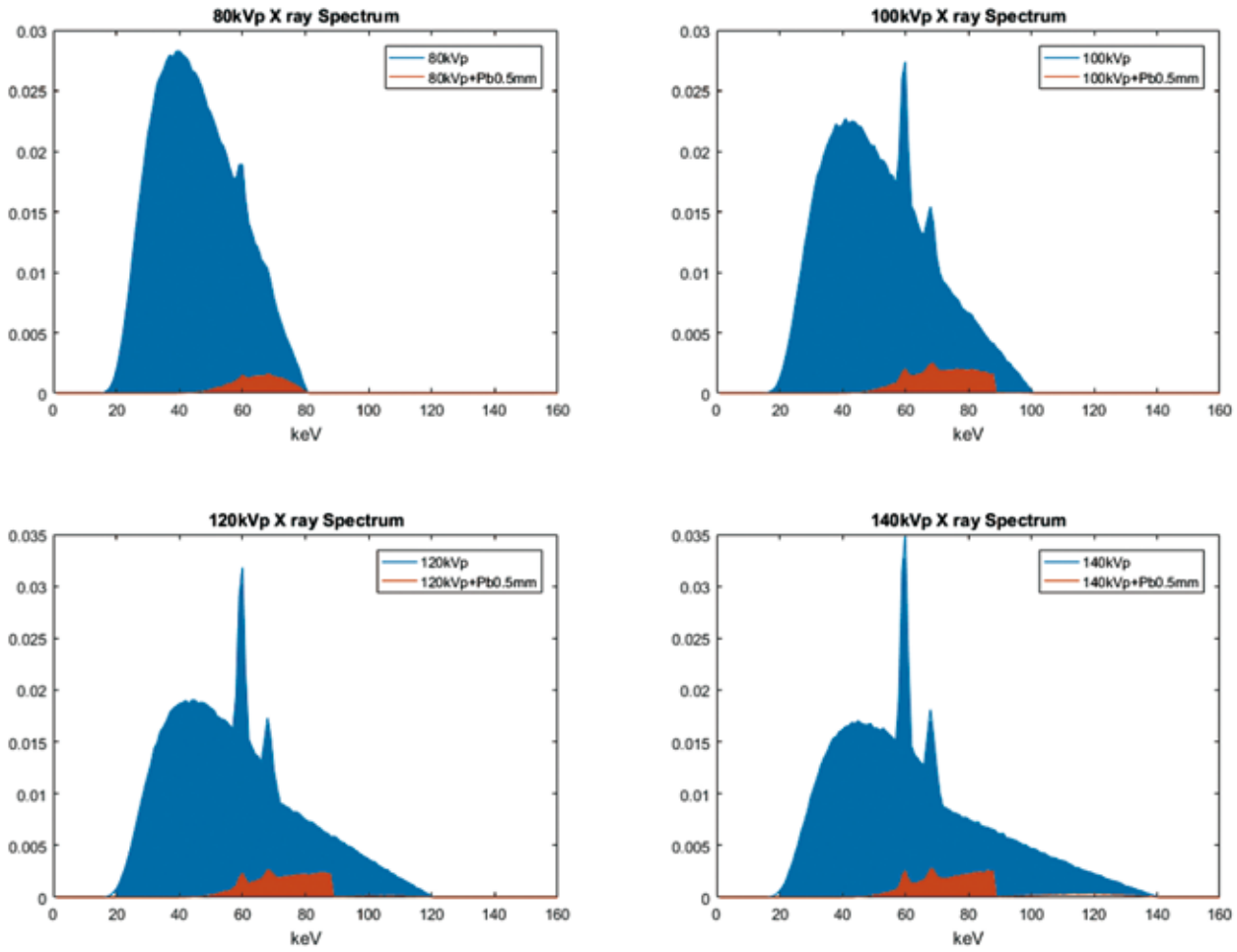

Figure 2. Simulation x-ray spectrum with and without lead shielding.

phantom in each X-ray simulation were showed as Table 1. The lead plate with a thickness of 0.5 mm effectively reduces the radiation dose to less than one tenth.

The single energy gamma ray simulation shows a different result. We plot the single energy gamma photon dose deposition along the depth of the water absorber as Figure 4. Total absorbed dose within the water phantom in each X-ray simulation were showed as Table 2.

Discussion

Lead aprons are used in medical facilities to protect workers and patients from unnecessary x-ray radiation exposure from diagnostic radiology procedures. A lead apron is a protective garment which is designed to shield staff's body from harmful radiation, usually in the context of medical imaging [9]. The most common lead protective clothing in the radiology department is the lead apron with a lead equivalent thickness of 0.5 mm [10]. Our Monte Carlo software simulation results show that 0.5 mm thickness of lead can effectively block those X-rays commonly used in general radiological image scans. Lead aprons are the primary radiation protective garments used by personnel during fluoroscopy. The radiation protection provided by a lead apron is approximately the same as 0.25 to 1mm thick lead. In previous research, an apron with 0.5-mm thickness can attenuate approximately 90% or more of the scatter radiation [11]. And lead glasses with 0.5 or 0.75 mm thickness can reduce more than 95% of scatter radiation

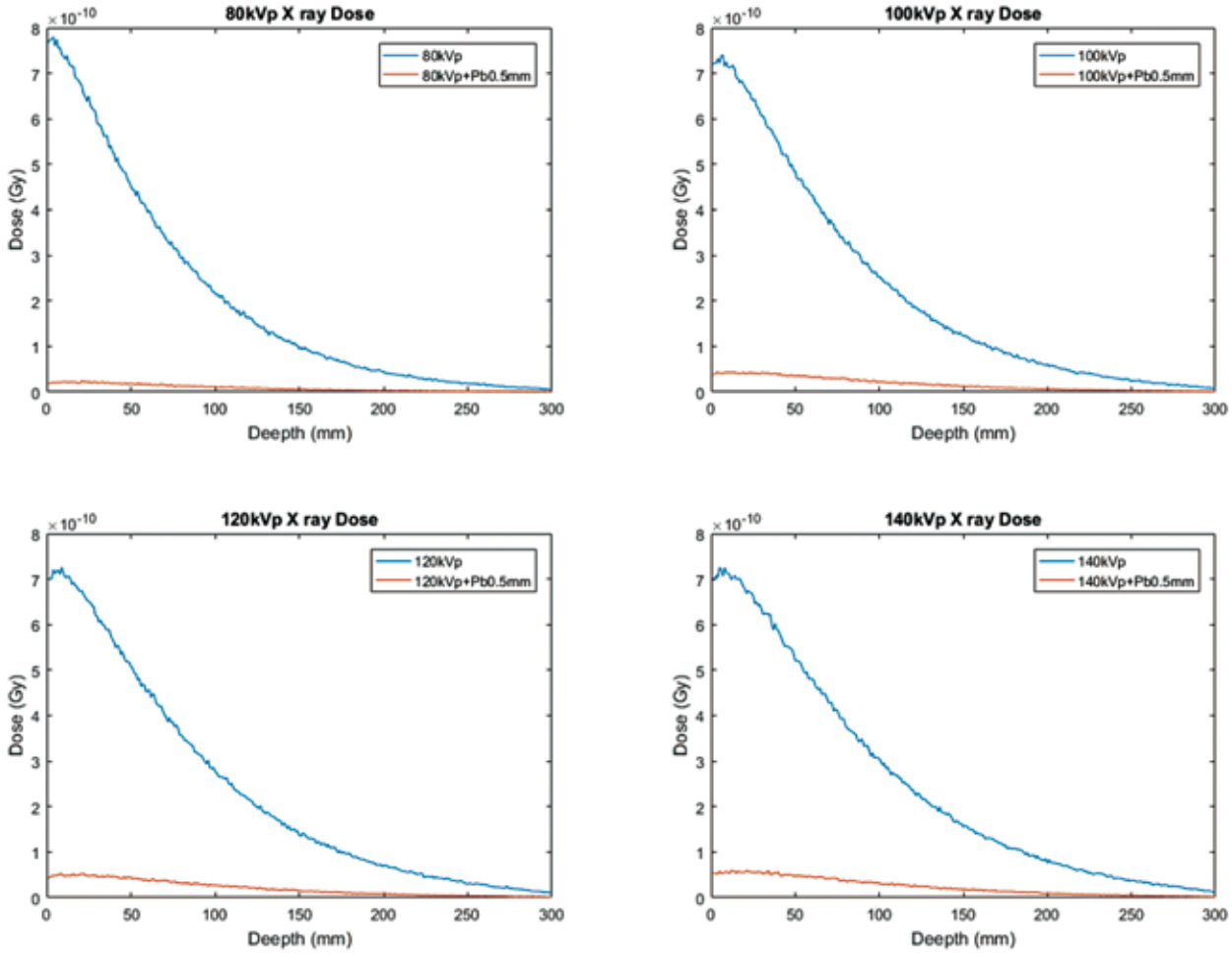

Figure 3. The absorbed dose in water cube calculated by GATE 7.2 with 80, 100, 120, 140 kVp x-ray.

Table 1. Total absorbed dose within the water phantom in X ray simulation

	Total absorbed dose within the water phantom		
Tube voltage	Direct irradiation (Gy)	With Pb 0.5 mm shielding (Gy)	Dose remain
80 kVp	6.05×10^{-8}	2.47×10^{-9}	4.08%
100 kVp	6.53×10^{-8}	5.11×10^{-9}	7.81%
120 kVp	6.96×10^{-8}	6.10×10^{-9}	8.76%
140 kVp	7.35×10^{-8}	7.09×10^{-9}	9.65%

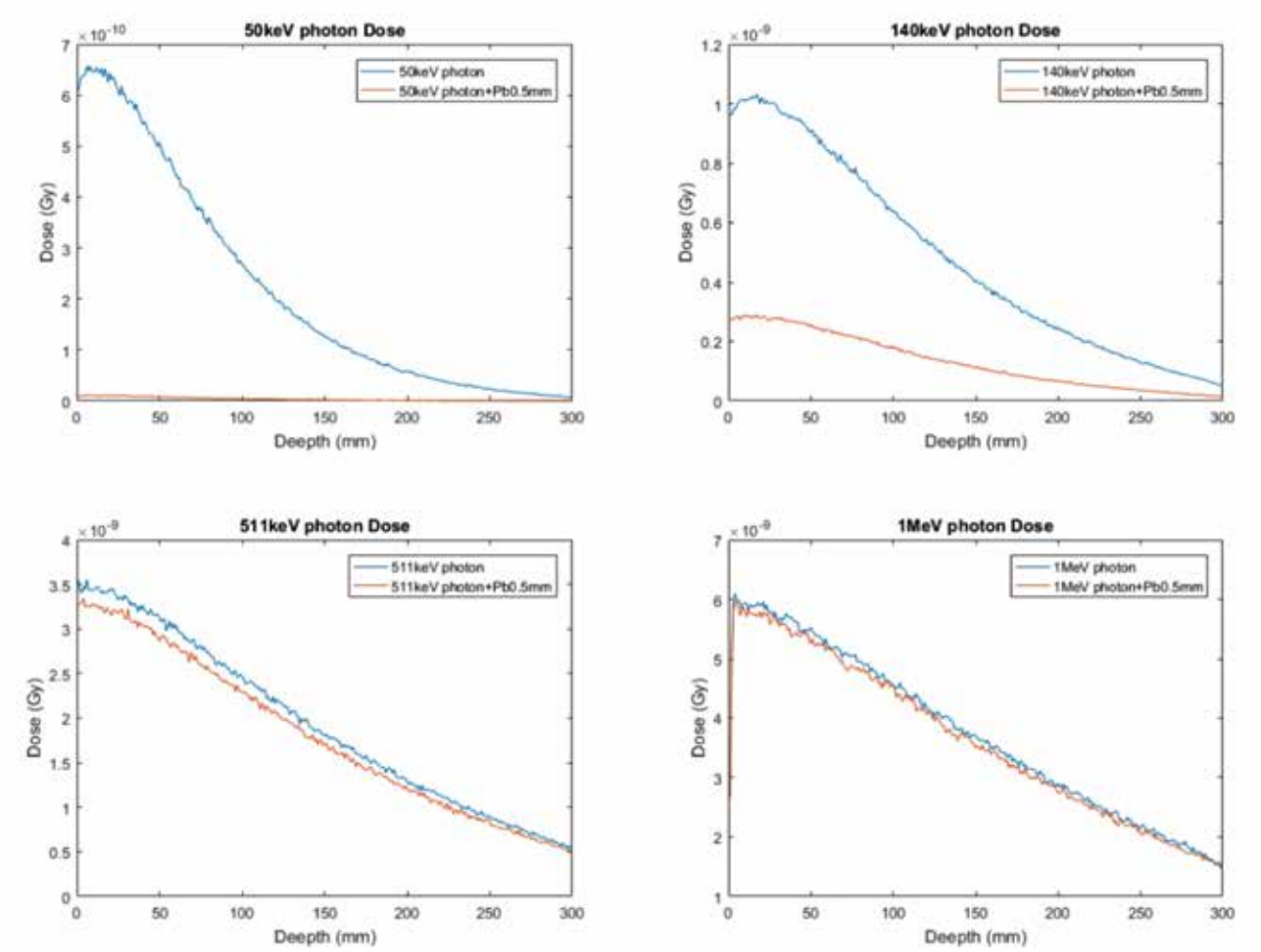

Figure 4. The absorbed dose in water cube calculated by GATE 7.2 with 50 keV, 140 keV, 511 keV, 1 MeV single energy gamma ray.

Table 2. Total absorbed dose within the water phantom in gamma ray simulation

	Total absorbed dose within the water phantom		
Photon Energy	Direct irradiation (Gy)	With Pb 0.5 mm shielding (Gy)	Dose remain
50 keV	6.51×10^{-8}	1.04×10^{-9}	1.59%
140 keV	1.43×10^{-7}	3.96×10^{-8}	27.76%
511 keV	5.79×10^{-7}	5.42×10^{-7}	93.54%
1 MeV	1.12×10^{-6}	1.09×10^{-6}	97.25%

[11]. The simulation data of the lead apron is consistent with previous research results.

The photon energy received in the nuclear medicine department is high than radiology department. During the tracer injection and certain procedures, workers will be exposed to radiation. The simulation data of this study confirms that under the irradiation of 140 keV photons of ^{99m}Tc, the lead apron with lead equivalent thickness of 0.5 mm can still reduce the dose to the of 30%. Lead apron can still be used as a protective tool when it is necessary to contact ^{99}mTc isotope operation.

During the PET scan operation, staff will be exposed to the 511 keV photon exposure. High photon energy also enables gamma rays to penetrate materials. In our simulation result, through the 0.5 mm lead plate, 511 keV photons will still cause almost 94% of the dose without shielding. The lead apron with lead equivalent thickness of 0.5 mm shows poor protection on high-energy photon exposure. When the photon energy reaches 1 MeV, the 0.5 mm lead plate has almost no protective effect.

An alternate way to compare the shielding requirements for X-ray and high energy gamma ray is to compare the half-value layer (HVL). The HVL is that thickness of material that will decrease the amount of exposure by one-half. The HVL for 511 keV photons in lead is 4.02 mm for photons [12]. The HVL for 50, 70, 100, 150 kVp X-ray in lead were 0.06, 0.17, 0.27, 0.3 mm [13]. As expected, the HVL for positron emitters is about 13 to 66 times greater than for X-ray. If you want to achieve the same protective effect, positron radiography staff must wear 13 lead aprons. That is a very heavy weight beyond the human could ever lift. Anecdotal experience has suggested that back pain in radiologists may result from extensive wearing of lead aprons [14]. Staffs in PET scanning department should use fixed lead shielding plate or minimizing exposure time, maximizing distance from the radiation source to reduce radiation exposure.

Conclusion

The simulation data shows that the lead clothing, commonly used in clinical practice with an equivalent thickness of 0.5 mm, has a very good protective effect on X-ray irradiation of 80, 100, 120, 140 kVp, and the staff of traditional radiation inspection units should indeed wear protection. The photon energy of the radioisotope used by the nuclear medicine department is higher, and the protective effect of lead clothing with a lead equivalent thickness of 0.5 mm is not ideal. For positron imaging 511 keV high-energy photons, the protection of lead plates with a thickness of more than 4mm is required to achieve 50% of the protection effect. In practice, it is impossible to wear such a thickness of lead coat protection. It should be considered to optimize the work process to reduce exposure time and sufficient thickness of lead bricks and lead plates should be considered. The lead apron is only effective when it matched with the appropriate radiation energy and is used in a safe and regularly inspected environment.

Reference

1. Shapiro, J., *Radiation Protection: A Guide for Scientists, Regulators, and Physicians*. 2002: Harvard University Press.
2. Bushberg, J. T., et al., *The Essential Physics of Medical Imaging*. 2011: Wolters Kluwer Health.
3. Waterstram-Rich, K. M. and D. Gilmore, *Nuclear Medicine and PET/CT - E-Book: Technology and Techniques.* 2016: Elsevier Health Sciences.
4. Bailey, D. L., et al., *Positron Emission Tomography: Basic Sciences.* 2005: Springer London.
5. R. Davila-SantiniArthurOlson, T. F. P., *Radiation Physics and Radiation Safety*, in *Endovascular Surgery.* 2011, Elsevier Inc. p. 27-39.
6. Jan, S., et al., GATE: *a simulation toolkit for PET and SPECT*. Physics in Medicine & Biology, 2004. 49(19): p. 4543.
7. Jan, S., et al., *GATE V6: a major enhancement of the GATE simulation platform enabling modelling of CT and radiotherapy.* Physics in Medicine & Biology, 2011. 56(4): p. 881.
8. Liebel, F., et al., *Irradiation of skin with visible light induces reactive oxygen species and matrix-degrading*

enzymes. Journal of Investigative Dermatology, 2012. 132(7): p. 1901-1907.

9. Miller, D. L., et al., *Occupational radiation protection in interventional radiology: a joint guideline of the Cardiovascular and Interventional Radiology Society of Europe and the Society of Interventional Radiology*. Cardiovascular and interventional radiology, 2010. 33(2): p. 230-239.
10. Oyar, O. and A. Kislalioglu, *How protective are the lead aprons we use against ionizing radiation?* Diagnostic and Interventional Radiology, 2012. 18(2): p. 147.
11. Schueler, B. A., *Operator shielding: how and why*. Techniques in vascular and interventional radiology, 2010. 13(3): p. 167-171.
12. Dell, M. A., *Radiation safety review for 511-keV emitters in nuclear medicine.* Journal of nuclear medicine technology, 1997. 25(1): p. 12-17.
13. Kelley, J. P. and E.D. Trout, *Broad-beam attenuation in lead for X rays from 50 to 300 kVp*. Radiology, 1972. 104(1): p. 171-175.
14. Moore, B., et al., *The relationship between back pain and lead apron use in radiologists*. AJR. American journal of roentgenology, 1992. 158(1): p. 191-193.

以蒙地卡羅模擬實驗展示鉛衣屏蔽效果

柴發順* 江泰林 歐玲君 李正輝

新光吳火獅紀念醫院正子中心

前 言

時間、距離、屏蔽，是體外輻射防護的 TSD 三原則。在傳統放射線檢查單位，通常採用鉛衣作爲輻射防護手段。在核子醫學部門所使用放射性同位素的光子能量比診斷中傳統使用的 X 射線能量高得多。因此在相同鉛當量下的鉛衣是否能爲核子醫學部門的工作人員提供適當的輻射防護令人質疑。本研究採用蒙地卡羅模擬實驗來驗證及展示鉛當量厚度爲 0.5 mm 鉛衣的屏蔽效果。

材料與方法

採用 GATE 軟體模擬 50 keV、140 keV、511 keV、1 MeV 單能光子及球管電壓爲 80、100、120、140 kVp 的 X 光，照射 30 × 30 × 30 cm 水假體。分別模擬光束直接照射，以及使用 0.5 mm 厚度鉛屏蔽下照射 10^6 光子的劑量分布。紀錄每 1 mm 厚度水中的劑量 (Dose)，單位爲格雷 (Gy)。

實驗結果

不使用鉛屏蔽情況下，對於管電壓爲 80、100、120、140 kVp 的 X 光照射水假體的輻射劑量分別爲 6.05×10^{-8}、6.53×10^{-8}、6.96×10^{-8}、7.35×10^{-8} 格雷 (Gy)，使用 0.5 mm 鉛板防護的劑量 2.47×10^{-9}、5.11×10^{-9}、6.10×10^{-9}、7.09×10^{-9} 格雷 (Gy)。使用鉛板防護後的照射分別爲不使用防護時的 4.08%, 7.81%, 8.76%, 9.65%，對 X 光的防護效果顯著。在 50 keV、140 keV、511 keV、1 MeV 單能光子照射下，水假體的輻射劑量分別爲 6.51×10^{-7}、1.43×10^{-7}、5.79×10^{-7}、1.12×10^{-6} 格雷 (Gy)。使用 0.5 mm 鉛板防護的劑量則爲 1.04×10^{-9}、3.96×10^{-8}、5.42×10^{-7}、1.09×10^{-6} 格雷 (Gy)。使用鉛板防護後的照射劑量分別爲不使用防護時的 1.59%、27.76%, 93.54%, 97.25%，對 511 keV、1 MeV 單能光子的防護效果不佳。

結 論

模擬數據顯示臨床常用鉛當量厚度爲 0.5 mm 鉛衣對於 80, 100, 120, 140 kVp 的 X 光照射具有非常良好的防護效果，傳統放射線檢查單位工作人員應確實穿戴防護。核子醫學部門所使用放射性同位素的光子能量較高，鉛當量厚度爲 0.5 mm 鉛衣防護效果不理想。針對正子造影 511 keV 高能光子需要 4 mm 以上厚度的鉛板防護達到 50% 的防護效果，實務上無法穿戴如此厚度的鉛衣防護，應考慮優化工作流程減少暴露時間及使用足夠厚度的鉛磚、鉛板防護。

關鍵詞：鉛衣、蒙地卡羅模擬、X 光、輻射劑量、輻射防護

核醫技學誌 2020;17:19-27

接受日期：2020 年 7 月 27 日
通訊作者：柴發順
單位：新光吳火獅紀念醫院正子中心
聯絡方式：台北市士林區文昌路 95 號 新光吳火獅紀念醫院正子造影中心
電子郵件：T005629@ms.skh.org.tw

^{99m}Tc-MDP Bone Scintigraphy and SPECT/CT Manifestations in Patient with Leiomyoma of the Uterus: A Report of Two Cases

Hsiu-Lan Chu[1], Hui-Chen Yu[2], Chun-Ying Sung[3], Ya-Wen Chuang[1], Chih-Ting Liu[1,3*]

[1]*Department of Nuclear Medicine, Kaohsiung Medical University Hospital, Kaohsiung Medical University, Kaohsiung, Taiwan*
[2]*Department of Medicine Imaging, Kaohsiung Medical University Hospital, Kaohsiung Medical University, Kaohsiung, Taiwan*
[3]*Department of Medical Imaging and Radiological Sciences, College of Health Science, Kaohsiung Medical University, Kaohsiung, Taiwan*

Abstract:

The ^{99m}Tc-methylene diphosphonate (^{99m}Tc-MDP) whole-body bone scan can help diagnose a number of bone conditions, including cancer of the bone or metastasis, location of bone inflammation and fractures, stress fractures and bone infection. We share two patient cases. One patient had a past history of breast cancer and the other had a past history of thyroid cancer. They underwent a follow-up ^{99m}Tc-MDP whole-body bone scan. However, the occasional extraskeletal 99mTc-MDP uptake in the pelvis was displayed; therefore, SPECT/CT imaging was acquired following the local planar image. Uterine leiomyoma was impressed.

Key words: ^{99m}Tc-MDP whole-body bone scan, SPECT/CT, Uterine leiomyoma

J Nucl Med Tech 2020;17:29-32

Received 2019/10/12
Corresponding author: Chih-Ting Liu
Department of Nuclear Medicine, Kaohsiung Medical University Hospital, Kaohsiung Medical University, Kaohsiung, Taiwan
Address: No. 100, Tzyou 1st Road Kaohsiung 807, Taiwan, R.O.C
Tel: 886-7-3121101 ext. 7154 E-mail: 980027@ms.kmuh.org.tw

Introduction

Uterine leiomyomas are an important problem in women's health [1], occurring from the overgrowth of smooth muscle and connective tissue in the uterus [2], and ranging from sizes small enough to not be palpable or visible by ultrasonography to one large enough to distort a woman's abdominal contour mimicking pregnancy. ^{99m}Tc-methylene diphosphonate (^{99m}Tc-MDP) whole-body bone scan can help diagnose a number of bone conditions, including cancer of the bone or metastasis, location of bone inflammation and fractures, stress fractures and bone infection. SPECT/CT can provide not only functional information but also anatomical information. We share two cases with occasional extraskeletal uptake of uterine leiomyoma in the pelvis.

Case reports

We share two patients with impression of uterine leiomyoma on ^{99m}Tc-MDP whole-body bone scan and SPECT/CT imaging. One patient had a past history of breast cancer and the other had a past history of thyroid cancer. They received a follow-up ^{99m}Tc-MDP whole-body bone scan. The bone scan was performed three hours after an intravenous injection of 20 mCi ^{99m}Tc-MDP.

The first patient was a 72-year-old woman and had a past history of infiltrating duct carcinoma of the right breast. Bone imaging showed low probability of bone metastasis.

However, the mild abnormal accumulation of radiotracer was shown in the pelvic cavity (arrow in Figure 1A). SPECT/CT imaging of the pelvis was acquired following the local planar image. The calcification spots in the uterus were also demonstrated on SPECT/CT imaging (arrow in Figure 1B) and uterine leiomyoma was impressed.

The second patient was a 55-year-old woman and had a past history of thyroid papillary carcinoma. Bone imaging showed low probability of bone metastasis. However, the focal extraosseous accumulation of radiotracer was shown in the pelvic cavity (arrow in Figure 2A). SPECT/CT imaging of the pelvis was acquired following the local planar image. SPECT/CT imaging demonstrated radiotracer accumulation around large uterine leiomyomas with dystrophic calcifications (arrow in Figure 2B).

Discussion

The accumulation of ^{99m}Tc-MDP is by both chemical adsorption onto the surface of the hydroxyapatite in bone and incorporation into the crystalline structure of hydroxyapatite [3]. The advantages of ^{99m}Tc-MDP bone scintigraphy include high sensitivity in detecting bone metastasis [4] and the ability to rapidly survey the entire skeleton.

In our two patients, the soft tissue accumulation of ^{99m}Tc-MDP in the pelvic cavity was shown on the planar image. SPECT/CT of pelvis was performed for these two patients and the area with ^{99m}Tc-MDP accumulation was shown to demonstrate uterine leiomyoma with calcification of solid mass.

The major limitation of ^{99m}Tc-MDP bone scintigraphy is its non-specificity. The soft tissue accumulation of ^{99m}Tc-MDP on bone scans is occasionally seen, and the etiologies of soft-tissue uptake, organized according to mechanisms of accretion: (1) metastatic calcification, (2) dystrophic calcification, (3) metabolic uptake, and (4) compartmental sequestration [5]. Calcium deposition in the soft-tissue can be found in a variety of disease processes (such as ischemia, necrosis, metastatic calcification in renal failure, or

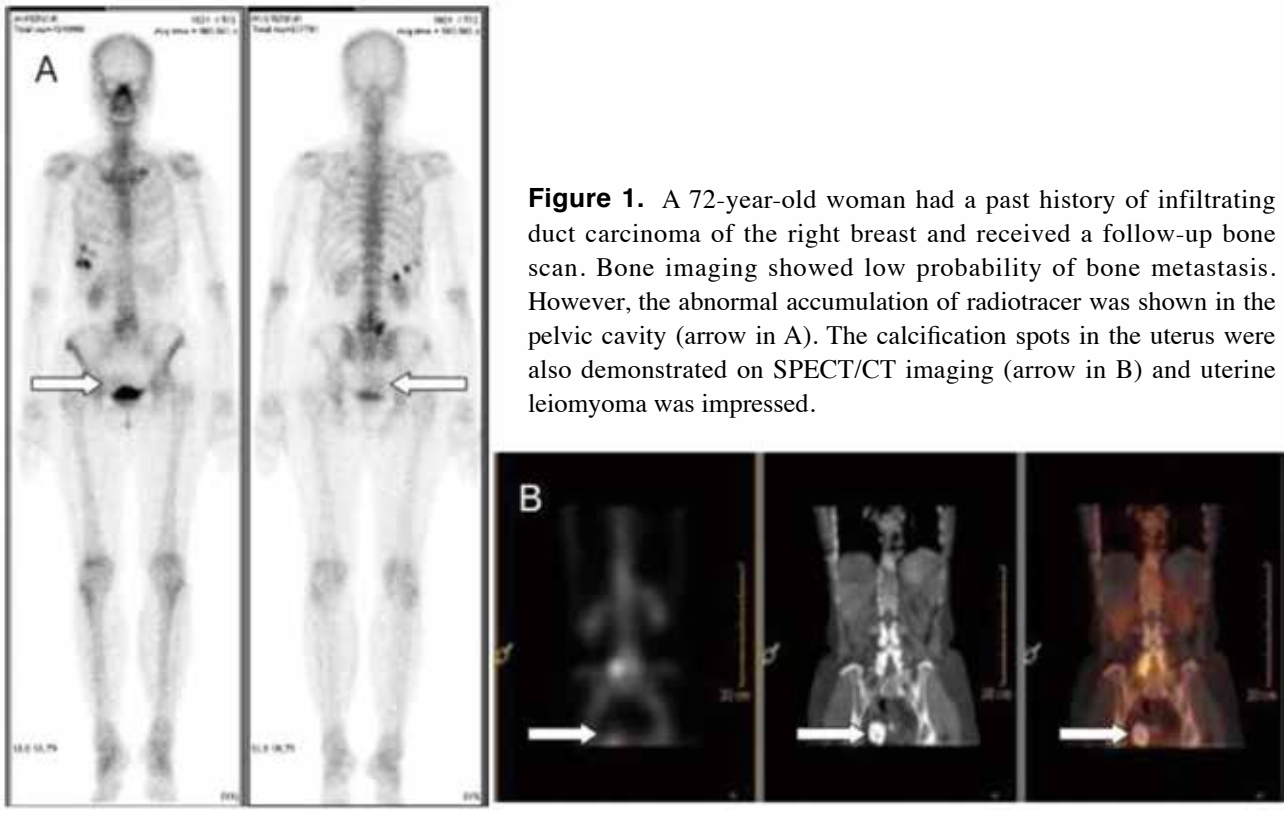

Figure 1. A 72-year-old woman had a past history of infiltrating duct carcinoma of the right breast and received a follow-up bone scan. Bone imaging showed low probability of bone metastasis. However, the abnormal accumulation of radiotracer was shown in the pelvic cavity (arrow in A). The calcification spots in the uterus were also demonstrated on SPECT/CT imaging (arrow in B) and uterine leiomyoma was impressed.

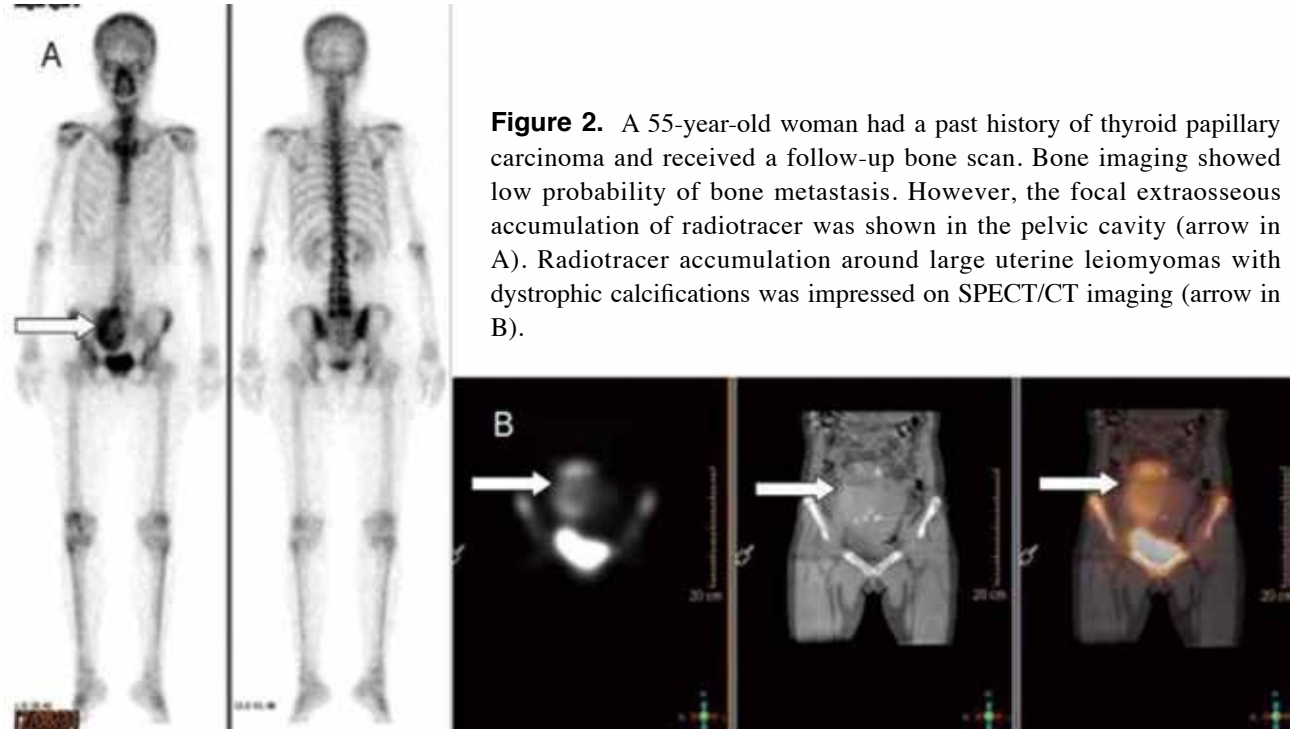

Figure 2. A 55-year-old woman had a past history of thyroid papillary carcinoma and received a follow-up bone scan. Bone imaging showed low probability of bone metastasis. However, the focal extraosseous accumulation of radiotracer was shown in the pelvic cavity (arrow in A). Radiotracer accumulation around large uterine leiomyomas with dystrophic calcifications was impressed on SPECT/CT imaging (arrow in B).

hypercalcemia of any cause), it is conceivable to find uptake of the bone radiotracer in any organ in the body [6]. CT findings of uterine leiomyomas and their secondary changes, including cystic degeneration, calcification, infection, necrosis, fatty degeneration, and sarcomatous degeneration [7].

In our two patients, CT imaging demonstrated soft tissue mass with calcifications and uterine leiomyoma was impressed. However, a reverse relationship was noted between severity of CT calcification and intensity of ^{99m}Tc-MDP accumulation. The first patient had a higher percentage of calcification in her uterine leiomyoma on SPECT/CT imaging and the ^{99m}Tc-MDP uptake was mild. In contrast, the second patient had a lower percentage of calcification in her uterine leiomyoma on SPECT/CT imaging and the ^{99m}Tc-MDP uptake was intense.

SPECT/CT is a very valuable modality for application in nuclear medicine; however, multimodality examinations result in increased radiation exposure dose and must be used under reasonable conditions that could improve the quality of diagnosis in the nuclear medicine department.

References

1. Laughlin SK, Stewart EA. Uterine leiomyomas: individualizing the approach to a heterogeneous condition. *Obstet Gynecol* 2011;117:396-403.
2. Medikare V, Kandukuri LR, Ananthapur V, Deenadayal M, Nallari P. The genetic bases of uterine fibroids; a review. *J Reprod Infertil* 2011;12:181-91.
3. Kanishi D. 99mTc-MDP accumulation mechanisms in bone. *Oral Surg Oral Med Oral Pathol* 1993;75:239-46.
4. Sahin E, Zincirkeser S, Akcan AB, Elboga U. Is (99m) Tc-MDP whole body bone scintigraphy adjuvant to (18) F-FDG-PET for the detection of skeletal metastases? *J buon* 2014;19:291-6.
5. Zuckier LS, Freeman LM. Nonosseous, nonurologic uptake on bone scintigraphy: atlas and analysis. *Semin Nucl Med* 2010;40:242-56.
6. Loutfi I, Collier BD, Mohammed AM. Nonosseous abnormalities on bone scans. *J Nucl Med Technol* 2003;31:149-53; quiz 54-6.
7. Casillas J, Joseph RC, Guerra JJ, Jr. CT appearance of uterine leiomyomas. *Radiographics* 1990;10:999-1007.

子宮肌瘤在 ^{99m}Tc-MDP 全身骨骼掃描與 SPECT/CT 影像上表現：兩位病例報告

朱秀蘭[1] 游慧貞[2] 宋純穎[3] 莊雅雯[1] 劉芝庭[1,3*]

[1] 高雄醫學大學附設中和紀念醫院核子醫學部
[2] 高雄醫學大學附設中和紀念醫院影像醫學部
[3] 高雄醫學大學醫學影像暨放射科學系

摘 要

^{99m}Tc-methylene diphosphonate (^{99m}Tc-MDP) 全身骨骼掃描可用於幫助診斷骨骼方面問題，例如骨癌或癌症骨轉移、骨骼發炎、骨折、應力性骨折和骨骼感染。我們分享兩位案例。一位病人過去病史具有乳癌，另一位病人過去病史具有甲狀腺癌。他們進行 ^{99m}Tc-MDP 全身骨骼掃描的追蹤。然而偶然在骨盆腔中有骨骼外攝取 ^{99m}Tc-MDP 的情況，因此在平面局部影像獲取後進行單光子電腦斷層掃描 / 電腦斷層掃描，影像被認爲是子宮肌瘤的表現。

關鍵詞：^{99m}Tc-MDP 全身骨骼掃描、單光子電腦斷層掃描 / 電腦斷層掃描、子宮肌瘤

核醫技學誌 2020;17:29-32

接受日期：2019 年 10 月 12 日
通訊作者：劉芝庭
單位：高雄醫學大學附設中和紀念醫院核子醫學部
住址：807 高雄市三民區自由一路 100 號
電話：886-7-3121101 轉 7154　電子郵件：980027@ms.kmuh.org.tw

Cancer Related Pulmonary Perfusion Defect Demonstrated by Tc-99m Macroaggregated Albumin Single-Photon Emission Computerized Tomography (SPECT)/Computed Tomography (CT)

Chun-Liang Kuo, Yu-Hung Chang*

Department of Nuclear Medicine, Hsinchu Mackay Memorial Hospital, Hsinchu, Taiwan

Abstract

A 68-year-old man with a history of left tonsil cancer, supraglottic cancer, open pulmonary tuberculosis and chronic kidney disease was suspected of pulmonary embolism. Poor renal function impeded computed tomography pulmonary angiography with iodinated contrast medium; ventilation-perfusion scan was ordered. However, we performed SPECT/CT instead because of its superior accuracy. Perfusion SPECT/CT showed large area of lobar perfusion defect in the right lung, possibly because cancer. Pulmonary tuberculosis was suspected etiology for the perfusion defect at the left lung apex. SPECT/CT provides more information than traditional planar ventilation-perfusion scan.

Key words: pulmonary embolism, chronic kidney disease, ventilation/perfusion scan, SPECT/CT

J Nucl Med Tech 2020;17:33-37

Received 2020/11/17
Corresponding author: Yu-Hung Chang
Department of Nuclear Medicine, Hsinchu Mackay Memorial Hospital, Hsinchu, Taiwan
Address: No. 690, Sec. 2, Guangfu Rd, East Dist, Hsinchu City, Taiwan (R.O.C.)
Phone: (886) 3-611-9595 #2299
Fax: (886) 3-611-5934 E-mail: 3053@mmh.org.tw

Figure 1.

A 68-year-old man with dyspnea was suspected of acute pulmonary embolism (PE). He had a history of left tonsil cancer, supraglottic cancer, open pulmonary tuberculosis (TB), and chronic kidney disease. Computed tomography (CT) pulmonary angiography (CTPA) with iodinated contrast medium was contraindicated owing to poor renal function. A ventilation-perfusion (V/Q) scan was referred to exclude PE. Technological advances in V/Q single-photon emission computerized tomography (SPECT) permits accurate diagnosis of PE without iodinated contrast administration and is more sensitive than CTPA and traditional planar V/Q scanning (1-2). Latest improvement, hybrid tomography, combines low-dose CT scan with V/Q SPECT scan. V/Q SPECT/CT presumably has the best diagnostic accuracy for PE among CTPA, planar scintigraphy, V/Q SPECT, and V/Q SPECT/CT (1-7). Moreover, perfusion only SPECT/CT can detect PE with high diagnostic efficiency (8-12). We chose perfusion SPECT/CT because of his history of open pulmonary TB.

We used a SPECT/CT system (Discovery NM/CT 670 pro, GE Healthcare, Haifa, Israel) for imaging. Planar perfusion images were acquired in the supine position with intravenous injection of 185 MBq (5 mCi) Tc-99m-macroaggregated albumin (Tc-99m-MAA). Image acquisition used low energy, high-resolution collimator, and images for 500,000 counts were obtained in the anterior, posterior, bilateral, right and left anterior, and posterior oblique views. Planar data used a functional imaging workstation (Xeleris

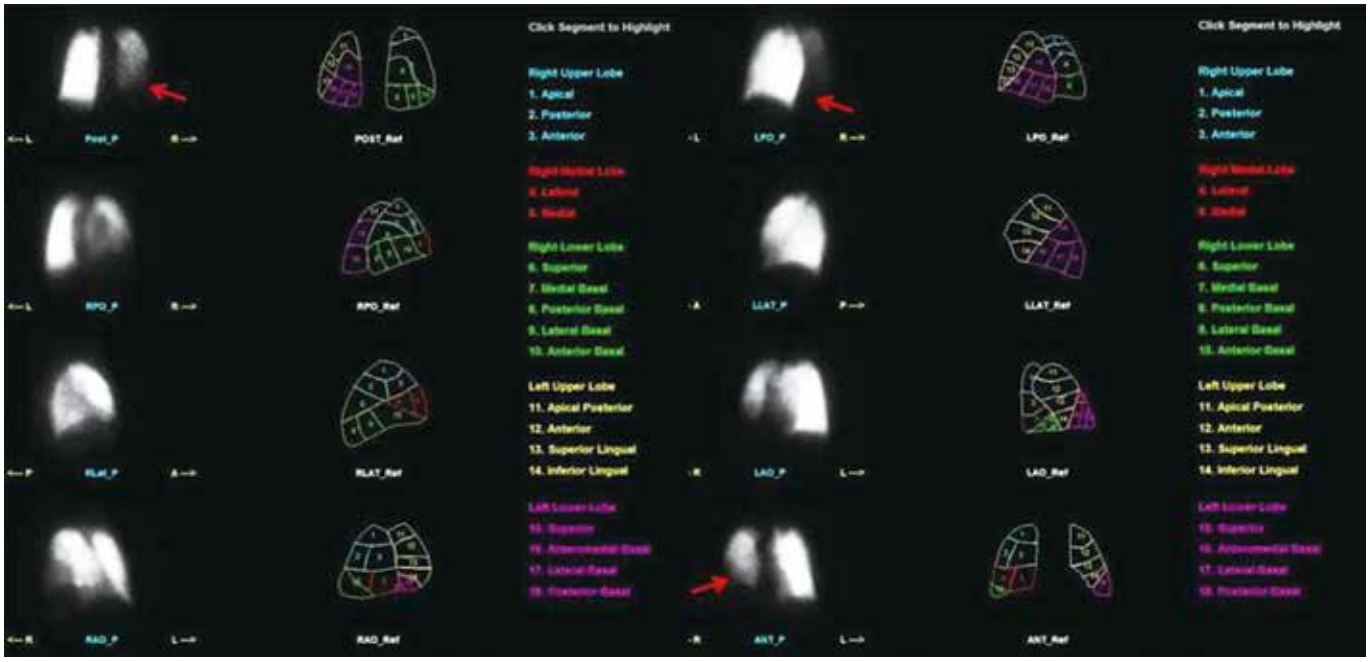

Figure 1.

version 3.1, GE Healthcare) for lung analysis. Fig. 1 shows extensive lobar perfusion defect at the right lung (red arrows) possibly caused by PE, secondary to tumor, radiation pneumonitis, airway infection, other insult, etc.

Figure 2.

A, Fusion images were acquired with GE hybrid SPECT/CT scanner, 30 minutes after planar perfusion imaging (CT parameters: 120 kVp, 20 mAs). A fusion program (Volumetrix MI) projected the scanned images onto the anatomical images obtained by CT to visualize 3-dimension colorized lung perfusion data. SPECT/CT images revealed possible cancer-induced right lower lung perfusion defect; therefore PE could not be excluded. B, Plain CT scan was performed with a 160 slice multi-detector CT scanner (AQUILON PRIME 160 TOSHIBA,

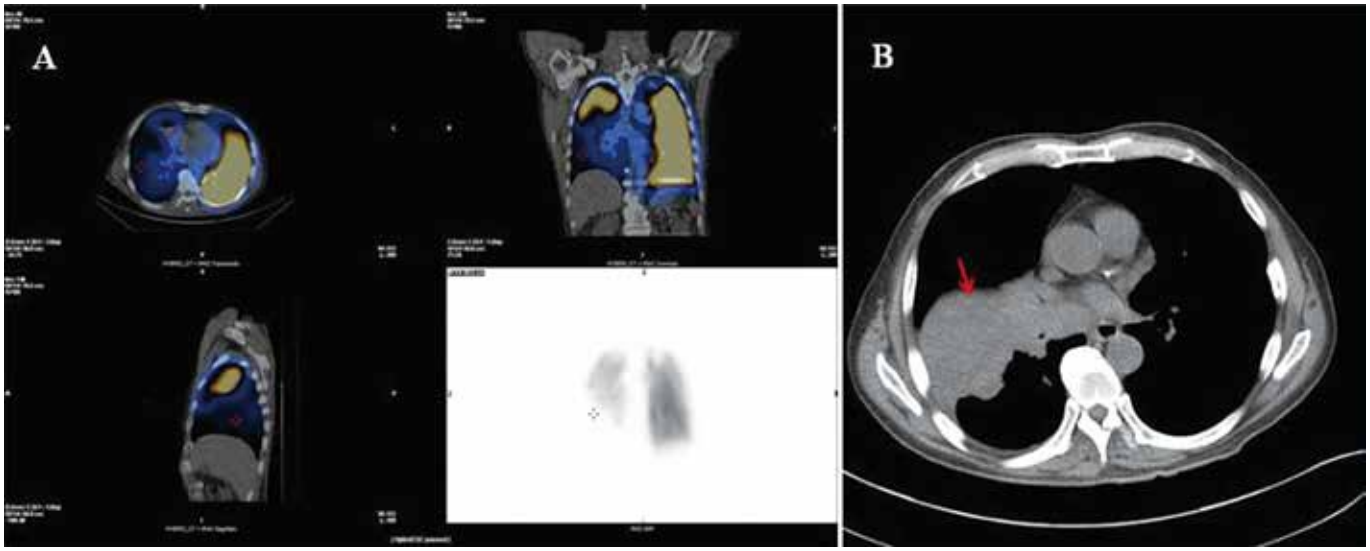

Figure 2.

JAPAN) with a scan area, 40 mm; slice thickness, 0.5 mm; tube voltage, 120 V; with automatic exposure control. The acquired image shows a large right lower lobe mass invading the right lower lobe bronchus and right inferior pulmonary vein, comparable to the malignant neoplasm of the lower lobe, right bronchus, or lung (red arrow).

Figure 3.

The left lung apex shows Tc-99m-MAA perfusion defect (A), corresponding to the cavitary lesion on chest radiograph (B, red arrow), possibly caused by TB. Acute PE is an important clinical complication with a high mortality rate (10- 30% if untreated, reducible 2 to 8% with treatment) (13). In contrast, excessive anticoagulant therapy can induce hemorrhage. Planar V/Q scan is optimal to diagnose PE when CTPA is contraindicated or unavailable. However, planar V/Q scanning has limitations. Planar imaging, a 2-dimensional technique has inherent limitations, especially due to overlapping anatomic segments. Assigning defects to specific lung segments is often difficult, potentially resulting in relatively high rate of indeterminate diagnosis. SPECT/CT is considered superior to SPECT, with the advantage of anatomic correlation (8-12). Herein, Tc-99m-MAA perfusion SPECT/CT is a feasible alternative to CTPA, and more informative than traditional planar V/Q scan, with or without SPECT.

References

1. Grüning T, Drake BE. V/Q SPECT in the diagnosis of pulmonary embolism. *BMJ*. 2013; 346:f1555.
2. Kan Y, Yuan L, Meeks JK, et al. The accuracy of V/Q SPECT in the diagnosis of pulmonary embolism: a meta-analysis. *Acta Radiologica*. 2015; 56:565-572.
3. Gutte H, Mortensen J, Jensen CV, et al. Detection of pulmonary embolism with combined ventilation-perfusion SPECT and low-dose CT: head-to-head comparison with multidetector CT angiography. *J Nucl Med*. 2009; 50:1987-1992.
4. Roach PJ, Schembri GP, Bailey DL. V/Q Scanning Using SPECT and SPECT/CT. *J Nucl Med*. 2013; 54:1588-1596.
5. Mortensen J, Gutte H. SPECT/CT and pulmonary embolism. *Eur J Nucl Med Mol Imaging*. 2014; 41:81-90.
6. Zhao Q, Yang H, Zhu X, et al. Comparison of SPECT/CT V/Q scan, CTPA & clinical probability of pulmonary embolism. *J Nucl Med*. 2018; 59(suppl 1):514.
7. Montecalvo N, Goldbach A, Ramakrishnan K, et al. Comparison SPECT/CT Perfusion/Ventilation Lung Scan to CTPA and to D-dimer Studies in Evaluation

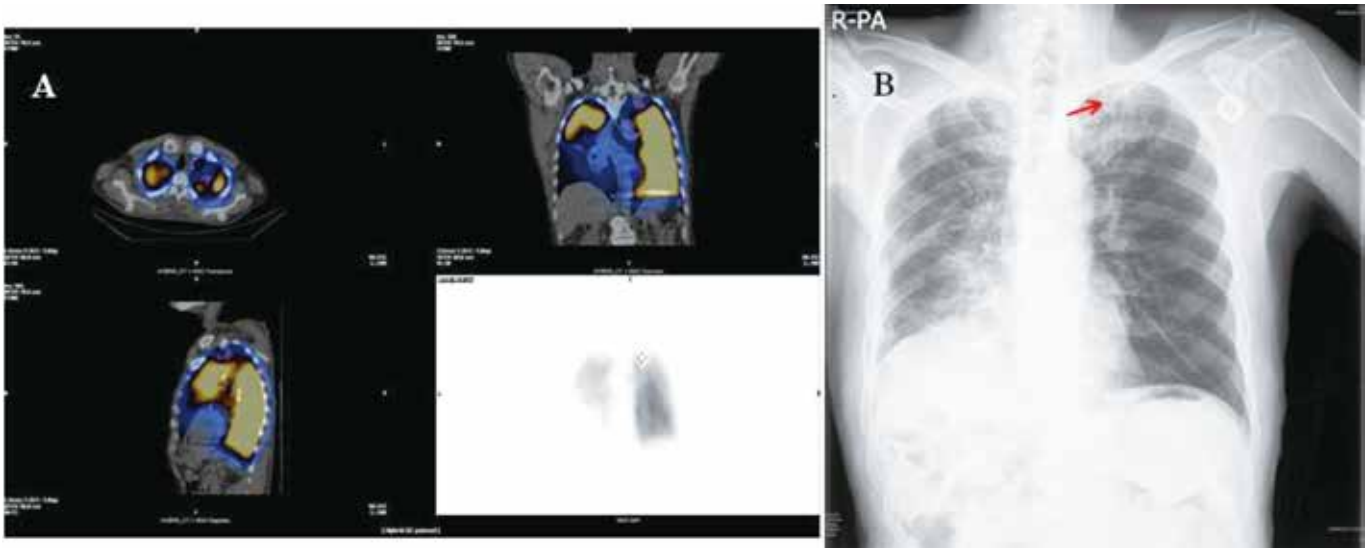

Figure 3.

of Patients with Acute Pulmonary Embolism: 5 year experience. *J Nucl Med*. 2018; 59(suppl 1):1565.

8. Suga K, Kawakami Y, Okada M, et al. Lung morphology-perfusion correlation on perfusion SPECT-CT fusion images in two cases of septic pulmonary embolism. *Clin Nucl Med*. 2010; 35:746-750.
9. Lu Y, Fox JJ. Acute pulmonary embolism detected by perfusion SPECT/CT masquerading as an intermediate probability planar V/Q scan. *Clin Nucl Med*. 2010; 35:941-943.
10. Lu Y, Lorenzoni A, Fox JJ, et al. Noncontrast perfusion single-photon emission CT/CT scanning: a new test for the expedited, high-accuracy diagnosis of acute pulmonary embolism. *Chest*. 2014; 145:1079-1088.
11. Mazurek A, Dziuk M, Witkowska-Patena E, et al. The utility of hybrid SPECT/CT lung perfusion scintigraphy in pulmonary embolism diagnosis. *Respiration*. 2015; 90:393-401.
12. Koukouraki SI, Hatzidakis AA, itrouska I, et al. Does lung perfusion scintigraphy continue to have a role in the clinical management of patients suspected of pulmonary embolism in the CT pulmonary angiography era? *Ann Nucl Med*. 2018; 32:709-714.
13. Goldhaber SZ, Visani L, De Rosa M. Acute pulmonary embolism: clinical outcomes in the International Co-operative Pulmonary Embolism Registry (ICOPER). *Lancet*. 1999; 353:1386-1389.

透過 SPECT/CT 於 ^{99m}Tc-MAA 肺灌注檢查證實肺癌侵犯所導致缺損之影像

郭俊良　張鈺弘 *

新竹馬偕紀念醫院核子醫學科

摘　要

一名 68 歲男子疑似肺栓塞的症狀，且他還患有左扁桃體癌，聲門上型癌，開放性肺結核與慢性腎病等病史。但由於腎功能不良，無法接受注射含碘離子造影劑之肺血管電腦斷層掃描檢查，所以臨床開立肺通氣 / 灌注掃描。然而，因 SPECT/CT 對診斷會有較高的準確度，此次檢查利用 SPECT/CT 來取代傳統平面的肺通氣 / 灌注掃描。透過肺灌注之 SPECT/CT 影樣結果清楚地顯示右肺有大面積肺葉灌注缺損，懷疑與癌症相關。另外，左肺頂端也發現灌注缺損，此缺損可能是由肺結核所引起的。故使用 SPECT/CT 檢查提供了比傳統核醫的平面通氣 / 灌注掃描更多的臨床信息。

關鍵詞：肺栓塞、慢性腎病、肺通氣 / 灌注掃描、SPECT/CT

核醫技學誌 2020;17:33-37

接受日期：2020 年 11 月 17 日
通訊作者：張鈺弘
新竹馬偕紀念醫院核子醫學科
地址：新竹市光復路二段 690 號
電話：(886) 3-611-9595 轉 2299　傳真：(886) 3-611-5934　電子信箱：3053@mmh.org.tw

False Positive Chest PET/CT Due to Arm Positioning in Patients with A History of Intercostal Surgery

Li-Chun Wu, Yu-An Yen, Chiang-Hsuan Lee*

Department of Nuclear Medicine, Chi Mei Medical Center, Tainan, Taiwan

Introduction

Whole-body positron emission tomography/computed tomography (PET/CT) can be performed with patients' arms positioned upward or downward and during tidal breathing. However, in patients with head and neck cancer, and melanoma and those who experience difficulty in lifting their arms, PET/CT images may be obtained with the arms positioned downward.

Case Presentation

We report two cases of thoracic artifact identified due to arm positioning and during tidal breathing in patients with a history of intercostal surgery. Both patients with cancer had a history of intercostal surgery, and recurrence was suspected in both cases. Moreover, when PET/CT images were obtained with the patients' arms positioned downward, incidental pleural-based masses were identified. However, the masses were less apparent when images were obtained with the patients' arms positioned upward, and no significant fluorodeoxyglucose uptake was noted. Diagnostic chest CT revealed that the size of the masses decreased, and they were consistent with thoracic artifact due to fibrosis.

Conclusions

To the best of our knowledge, no similar case has been reported to date, and this study highlights the importance of surgeries considering the possibility of occurrence of this problem to reduce the incidence of misdiagnosis and that resection is unnecessary.

Key words: PET/CT, Thoracic artifact, Pleural-based mass, Intercostal surgery, Tidal breathing

J Nucl Med Tech 2020;17:39-44

Received 2020/8/11
Corresponding author: Chiang-Hsuan Lee
Department of Nuclear Medicine, Chi Mei Medical Center, Tainan, Taiwan
Address: No. 901, Zhonghua Rd., Yongkang Dist., Tainan City 710, Taiwan (R.O.C.)
Phone: 886-6-281-2811 ext. 53575 E-mail: chlee4@ms45.hinet.net

Introduction

Patients with buccal cancer typically present with increased fluorodeoxyglucose (FDG) uptake, and in such conditions, metastasis to the lungs is most commonly observed. Positron emission tomography/computed tomography (PET/CT) has a high sensitivity in detecting distant metastases [1] and lung cancer [2,3].

To avoid the occurrence of streak artifact caused by the positioning of the arms downward [4,5], dual-point-time PET could be performed to improve and enhance sensitivity and specificity [6]. Our routine protocols are as follows. Initial whole-body imaging is performed from the top of the head to the feet with the arms positioned downward during tidal breathing using low-dose spiral CT without contrast [7,8].

Delayed imaging is performed in two steps [7,8]: (1) The head and neck with the arms positioned downward and (2) from the apex of the lungs to the mid-thigh with the arms positioned upward.

Herein, we report two cases of thoracic artifact identified due to arm positioning and during tidal breathing in patients with a history of intercostal surgery. To the best

of our knowledge, no similar case has been reported in the literature.

Case Presentation

Case 1

A 49-year-old man was diagnosed with T2N0M0 left buccal cancer 4 years prior to presentation, and he underwent surgical resection. Two years later, a left lung nodule was surgically removed via the left fifth intercostal space, and metastasis was pathologically confirmed.

Follow-up diagnostic chest CT revealed a new small nodule in the left lung. Recurrence was suspected and PET/CT was performed. The newly detected nodule showed no FDG uptake. However, the initial PET/CT images showed an incidental left lateral pleural-based mass abutting in the fifth intercostal space. This mass decreased in size and retreated into the space on the delayed PET/CT images, and no FDG uptake was observed on the initial or delayed PET images. In addition, the revised prior diagnostic chest CT image showed no abnormality at this site (Figure 1). Follow-up diagnostic chest CT image obtained after 3 months showed no abnormality at this site. Therefore, this mass was considered consistent with a fibrotic artifact identified due to the positioning of the arms downward and during tidal breathing.

Case 2

A 69-year-old man was diagnosed with T1bN0M0 right lung cancer 3 years prior to presentation. The nodule was surgically excised via the right seventh intercostal space, and adenocarcinoma was pathologically confirmed.

Based on the follow-up diagnostic chest CT, a new right upper lung nodule was detected. Recurrence was suspected, and PET/CT was performed that revealed no significant increase in FDG uptake. However, the initial PET/CT images showed an incidental right lateral pleural-based mass abutting in the seventh intercostal space. The size of the mass decreased and retreated into the space on the delayed PET/CT images, and a mild FDG uptake was observed on the initial PET/CT images. However, no more increase in FDG uptake was noted on the delayed PET/CT images. In addition, the revised prior diagnostic chest CT image showed less prominence at this site (Figure 2). The mass was consistent with thoracic artifact due to fibrosis that was attributed to prior surgical changes.

Discussion

Buccal cancer with lung metastasis is usually characterized by an increased FDG uptake; however, metastasis was unlikely to occur in the case 1 patient with left pleural-based mass without FDG uptake. The initial and delayed PET/CT images were obtained during tidal breathing and with different arm positions, which probably accounted for the observed changes in mass size. On prior diagnostic chest CT, we observed chest wall dilation during deep inspiration and a thin mass that retreated into the fifth intercostal space. Furthermore, the left lateral pleural-based mass was identical to that observed at the prior surgical site, which was consistent with prior intercostal surgical changes, such as subtle fibrosis.

Lung cancer is usually characterized by a significantly increased FDG uptake. In case 2, the right pleural-based mass had a mild FDG uptake on the initial PET/CT images, and no more increase in FDG uptake was observed on delayed PET/CT images. It was also consistent with an artifact caused by contracted fibrosis identified due to the positioning of the arms downward and during tidal breathing.

Diagnostic chest CT with the arms positioned upward and during full inspiration can dilate the chest. Thus, thoracic artifacts are not commonly identified. However, whole-body PET/CT images are usually obtained with the arms positioned downward and during tidal breathing. In addition, thoracic artifacts are more common in patients with a history of intercostal surgery.

Conclusion

In patients with a history of intercostal surgery, PET/CT images obtained with the arms positioned downward and during tidal breathing may reveal thoracic artifacts near the surgical site of the pleura. This study is helpful in prompting

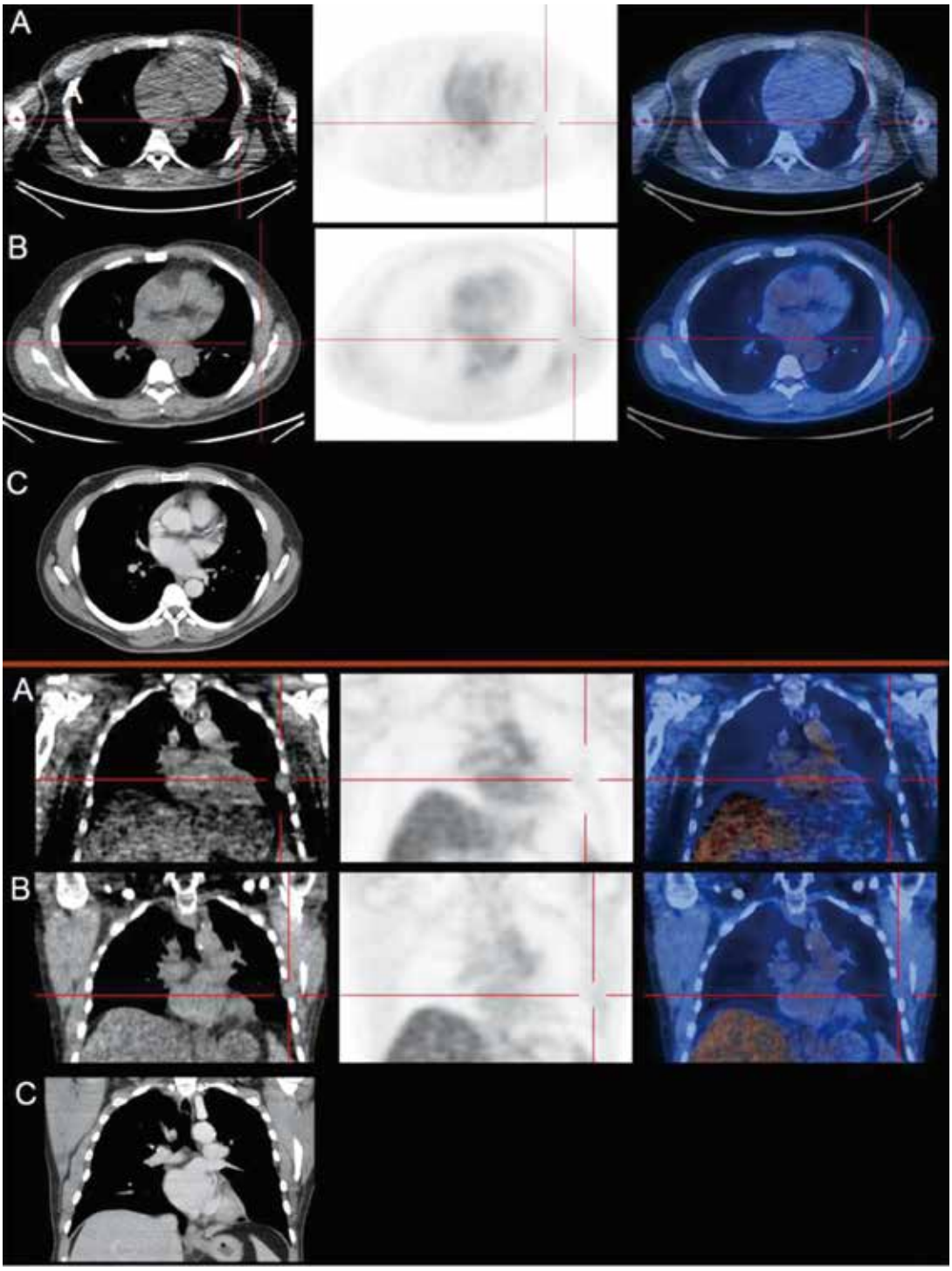

Fig. 1 Case 1: Axial (upper) and coronal (lower) positron emission tomography/computed tomography (PET/CT) images and diagnostic chest CT image. PET/CT images obtained with the arms positioned downward and during tidal breathing (A) show a mass (red crosshair); corresponding delayed images obtained with the arms positioned upward and during tidal breathing (B) shows that the lesion decreased in size and retreated into the fifth intercostal space. This mass does not show fluorodeoxyglucose uptake. Diagnostic chest CT (C) shows no abnormality at this site.

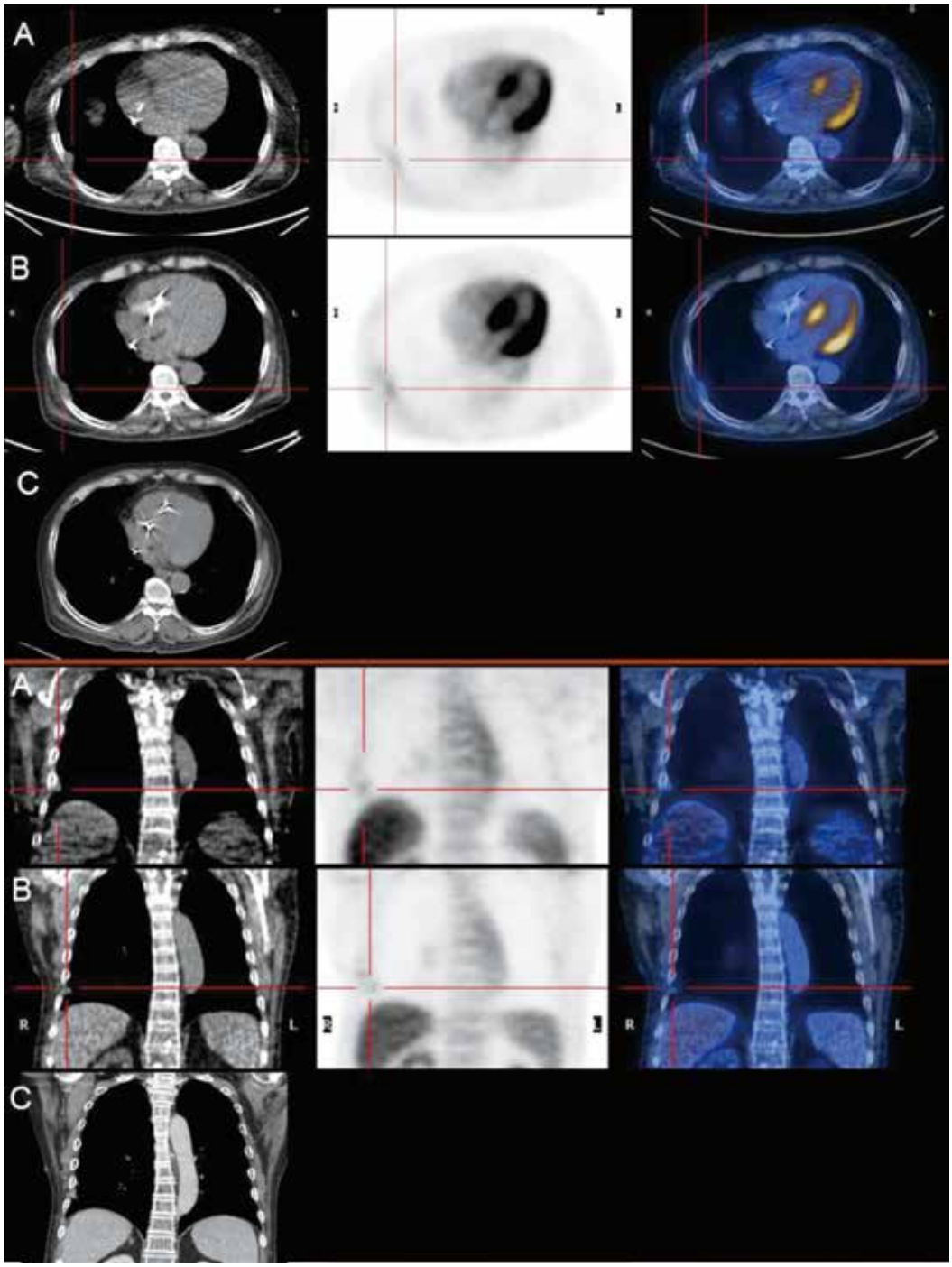

Fig. 2. Case 2: Axial (upper) and coronal (lower) positron emission tomography/computed tomography (PET/CT) images and diagnostic chest CT image. PET/CT images obtained with the arms positioned downward and during tidal breathing (A) show a mass (red crosshair); corresponding delayed images obtained with the arms positioned upward and during tidal breathing (B) shows that the lesion decreased in size and retreated into the seventh intercostal space. The mass decreased in size and retreated into the space on the delayed PET/CT images. However, mild FDG uptake is observed on the initial PET/CT images, and no significant increase in FDG uptake is noted on the delayed PET/CT images. Prior chest diagnostic chest CT (C) image shows less prominence at this site.

surgeries to identify this problem to reduce the incidence of misdiagnosis and resection may not be necessary.

References

1. Kim SY, Roh JL, Yeo NK, Kim JS, Lee JH, Choi SH, Nam SY (2007). Combined 18F-fluorodeoxyglucose-positron emission tomography and computed tomography as a primary screening method for detecting second primary cancers and distant metastases in patients with head and neck cancer. *Ann Oncol 18* (10):1698-1703. doi: 10.1093/annonc/mdm270
2. Herder GJ, Golding RP, Hoekstra OS, Comans EF, Teule GJ, Postmus PE, Smit EF (2004). The performance of(18)F-fluorodeoxyglucose positron emission tomography in small solitary pulmonary nodules. *Eur J Nucl Med Mol Imaging 31* (9):1231-1236. doi: 10.1007/s00259-004-1552-7
3. Nomori H, Watanabe K, Ohtsuka T, Naruke T, Suemasu K, Uno K (2004). Evaluation of F-18 fluorodeoxyglucose (FDG) PET scanning for pulmonary nodules less than 3 cm in diameter, with special reference to the CT images. *Lung Cancer 45* (1):19-27. doi: 10.1016/j.lungcan.2004.01.009
4. Barrett JF, Keat N (2004). Artifacts in CT: recognition and avoidance. *Radiographics 24* (6):1679-1691. doi: 10.1148/rg.246045065
5. Popilock R, Sandrasagaren K, Harris L, Kaser KA (2008). CT artifact recognition for the nuclear technologist. *J Nucl Med Technol 36* (2):79-81. doi: 10.2967/jnmt.107.047431
6. Schillaci O (2012). Use of dual-point fluorodeoxyglucose imaging to enhance sensitivity and specificity. *Semin Nucl Med 42* (4):267-280. doi: 10.1053/j.semnuclmed.2012.02.003
7. Beyer T, Antoch G, Muller S, Egelhof T, Freudenberg LS, Debatin J, Bockisch A (2004) Acquisition protocol considerations for combined PET/CT imaging. *J Nucl Med 45* Suppl 1:25s-35s
8. Boellaard R, Delgado-Bolton R, Oyen WJ, Giammarile F, Tatsch K, Eschner W, Verzijlbergen FJ, Barrington SF, Pike LC, Weber WA, Stroobants S, Delbeke D, Donohoe KJ, Holbrook S, Graham MM, Testanera G, Hoekstra OS, Zijlstra J, Visser E, Hoekstra CJ, Pruim J, Willemsen A, Arends B, Kotzerke J, Bockisch A, Beyer T, Chiti A, Krause BJ (2015). FDG PET/CT: EANM procedure guidelines for tumour imaging: version 2.0. *Eur J Nucl Med Mol Imaging 42* (2):328-354. doi: 10.1007/s00259-014-2961-x

曾有肋間手術史患者因手臂定位而導致 PET/CT 胸部僞陽性

吳麗君　顏玉安　李將瑄*

奇美醫療財團法人奇美醫院核子醫學科

前　言

全身正子掃描（PET / CT）可以在潮氣呼吸期間將患者的手臂向上或向下放置進行。但是，在患有頭頸癌和黑色素瘤的患者以及難以舉起手臂的患者中，可以將手臂向下放置來獲取 PET / CT 圖像。

病例報告

我們報告了 2 例因曾有肋間手術史患者的手臂位置和潮氣呼吸期間發現的胸部僞影。兩名癌症患者均具有肋間手術史，並且均懷疑復發。此外，當在患者手臂向下放置的情況下獲得 PET / CT 圖像時，可以識別出偶然的基於胸膜的腫塊。但是，當將患者的手臂向上放置而獲得圖像時，腫塊不太明顯，並且未發現明顯的氟 -18 去氧葡萄糖攝取。診斷性胸部 CT 顯示腫塊縮小，並且與纖維化引起的胸部僞影相符。

結　論

據我們所知，迄今爲止尚無類似病例的報導，本研究強調考慮該問題的發生以減少誤診的可能性以及不必要的手術。

關鍵字：PET / CT、胸廓僞影、胸膜腫塊、肋間手術、潮氣呼吸

核醫技學誌 2020;17:39-44

接受日期：2020 年 8 月 11 日
通訊作者 : 李將瑄
單位 : 奇美醫療財團法人奇美醫院核子醫學科
地址 : 台灣台南市永康區中華路 901 號 郵遞區號 71004
電話：06-2812811 分機 53575　電子信箱：chlee4@ms45.hinet.net